UNIVERSITY OF CYPRUS

Master Thesis

Design, Implementation and Experimental Testing of a Robotic Mechanism for Applications in Adaptive Architecture

LOUKAS GEORGIOU

DEPARTMENT OF MECHANICAL AND MANUFACTURING ENGINEERING

JUNE 2022

UNIVERSITY OF CYPRUS
DEPARTMENT OF MECHANICAL AND MANUFUCTURING ENGINEERING

Design Implementation and Experimental Testing of a Robotic Mechanism for Applications in the Adaptive Architecture

Loukas Georgiou

Thesis Supervisor
Dr. Eftychios Christoforou

The Diploma Thesis was submitted for partial fulfilment of the requirements for obtaining the Master's degree in Mechanical Engineering at the Department of Mechanical and Manufacturing Engineering

June 2022

Acknowledgments

First of all I want to thank my parents for the continuous support they offer me throughout my studies. Next, I would like to thank the supervisor of my dissertation Dr. Eftychios Christoforou for the guidance during my research project.

In conclusion, I would like to thank the special scientist Mr. Constantinos Sophocleous for the help he provided me for the implementation and construction of the robotic mechanism.

Abstract

A modern form in Adaptive Architecture is the buildings that have the ability to adapt their shape according to certain conditions, in order to achieve better use and better energy efficiency. In the present dissertation a method has been investigated, which combines a modular construction together with a corresponding control technique. For the study of these methods, their experimental validation on a small scale is important. In this context, the dissertation concerns the construction and optimization of an experimental system for this purpose. A robotic mechanism was designed and constructed. Simulations and experiments were used to demonstrate the applicability of the approach and investigate relevant details.

Contents

Figures

Appendices

Chapter 1

1 INTRODUCTION

1.1 Adaptive Architecture

Structures that are not fixed and can change their shape, position and orientation have great advantages that can contribute to achieving an innovative and flexible built environment. Compared to traditional fixed constructions, buildings that have the ability to be reconfigured provide unique opportunities, such as: (i) Optimizing user comfort by adjusting ventilation and lighting, (ii) Reduce of aerodynamic loads on the structure, (iii) Optimization of the use of space to serve different operational needs, (v) Optimization of the efficiency of a photovoltaic roof, (vi) shake off the snow of the roof, (vii) Providing unique aesthetic effects [1, 2].

Figure 1: 1) Adjustable roof suitable for sunlight, 2) Adjustable wing roof for air circulation, 3) Aesthetic building view, 4) Movable photovoltaic Wall, 5) Adjustable building shell.

The Adaptive Architecture is implemented offering a variety of alternative and flexible applications, as shown in Figure 1. The application of automatic control systems improves the efficiency of the building as it can respond dynamically to environmental stimuli such as sunlight and wind loads. Also, it is possible to make the best use of spaces by redefining its geometry. The geometry of the building can be completely changed, for example turning a pointed, tall and narrow building into a wide one with a semicircular roof. Shape adjustments may be carried out to accommodate changing needs of human activity or adapt in response to environmental stimuli [3, 4].

The majority of reconfigurable structures that have been developed and implemented to date, are based on integrated computing and the replacement of primary components with actuators, which often leads to increased structural weight, complex mechanisms, and energy inefficient operation. This work presents an approach, based on a reduced number of actuators, detached from the main structure, with the aim of maintaining minimum self weight, structural simplicity, and reduced energy consumption for temporary buildings.

1.2 Structural and control concept

A basic structural system consists of a parallel connection of planar multilink mechanisms, as shown in Figure 2. Interconnections between planar multilink mechanisms produce the complete skeleton structure. Each link connects with each other with joints and allows them to move together, while control action is transferred between them and the overall shape of the building changes accordingly. They also provide the building with structural stiffness in the longitudinal direction [5, 6]. Between the corresponding members of the planar linkages different elements can be installed including membranes, shades, and photovoltaic panels. Some reinforcing material also can be used such as carbon fibers panels or plexiglass. The following analyses focus on a single planar basic mechanism and its reconfigurations.

Figure 2: Planar multilink mechanism skeleton.

One methodology proposed for the control of adaptive structures is the coupled crank slider which involves a planar closed-chain systems [7]. This system consists of one actuated sliding block and two chains, one on either side. Each chain has links that are serially connected and is pinned to the ground. The joints that connect the links together have a rotational movement which is controlled by an installed brake. Appling the brakes

at the joints creates connected links that can be described as “effective links”. When there are three brakes released on each chain then the system becomes a “coupled effective crank-slider” (CECS) mechanism, as shown in Figure 3 for the horizontal setup and Figure 4 for the vertical setup. In this way the mechanism is a 1-degree of freedom system and the building is composed of a number of planar, closed-chain mechanisms, which change the overall shape of the building as they are adjusted. In order to reach the final configuration of the CECS mechanism can be used multiple intermediate reconfigurations. At each reconfiguration step one angle is adjusted to its final value and remains locked for the remaining process. When all joints are adjusted the reconfiguration process is completed. Motion planning involves alternative reconfiguration sequences, which should also consider singular configurations [8].

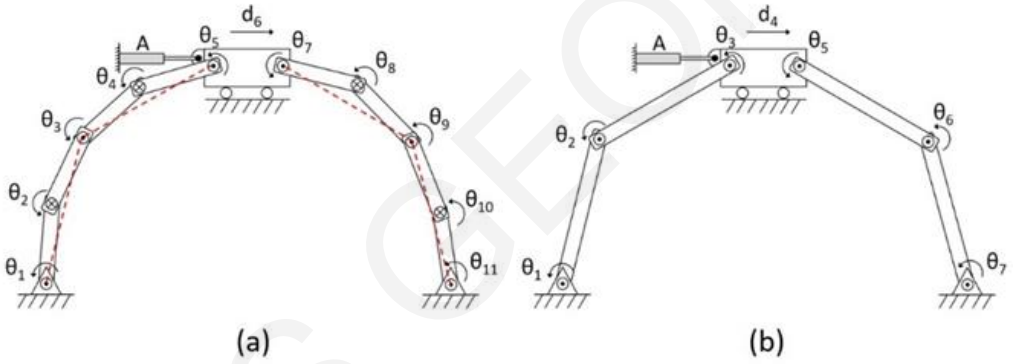

Figure 3: (a) The basic planar mechanism for horizontal motion and the control concept. (b) The corresponding coupled effective crank-slider mechanism. (⊗: locked joint, ⊙: unlocked joint, △: pivoted–to–the–ground joint, dashed lines represent effective links, A: linear actuator).

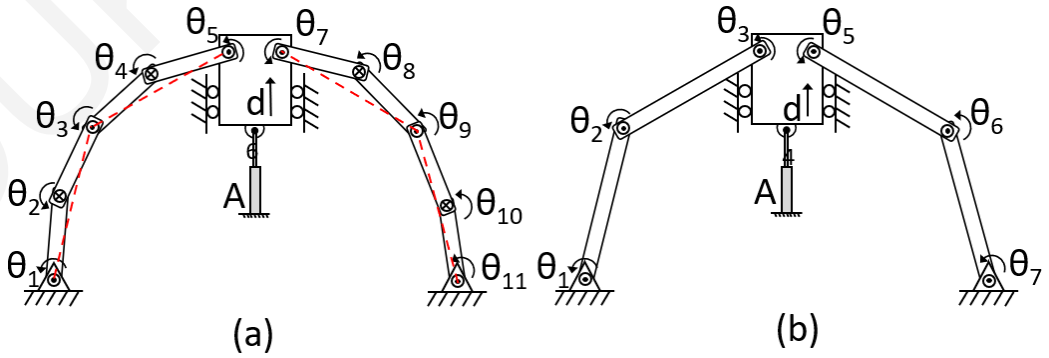

Figure 4: (a) The basic planar mechanism for vertical motion and the control concept. (b) The corresponding coupled effective crank-slider mechanism. (⊗: locked joint, ⊙: unlocked joint, △: pivoted–to–the–ground joint, dashed lines represent effective links, A: linear actuator).

The integration of thin-film photovoltaic modules on the spatial structure of the above reconfigurable building with regard to the solar irradiance and energy production were examined in [7]. An example of relevant simulation studies performed by our lab is shown in Figure 5.

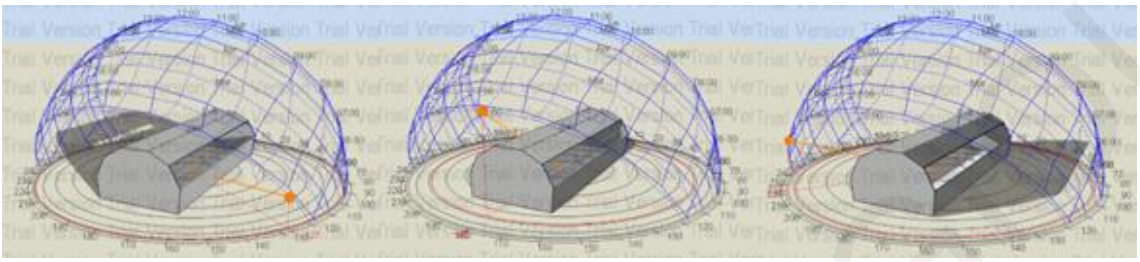

Figure 5: Example of solar gain and lighting simulation.

The following chapters contain the key to implementing them. Chapter 2 describes the mechanical and electronic members that comprise the robotic mechanism, the power supply and control boxes, giving a detailed description of each component. The programing code is described which written for testing and taking measurements from the robotic mechanism through the LabVIEW, as well as a brief summary of the card that connects to the computer. Next, chapter 3 “Simulation and Experimental Studies” contains the Motion Planning, Simulation and Experimental Study. Finally, chapter 4 contains the conclusions, recommendations for further work and possible future applications in which the methodology of the mechanism can be used.

Chapter 2

2 DESIGN AND PROTOTYPE DEVELOPMENT

2.1 Mechanical System

The robotic mechanism consists of many parts, as shown in Figure 6.

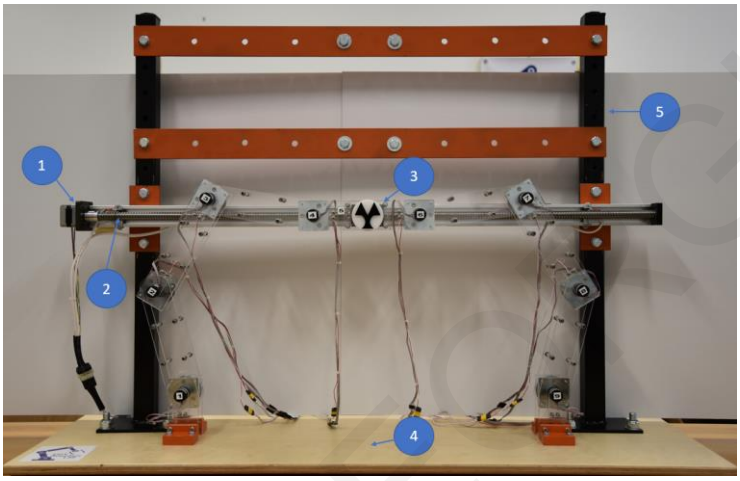

Figure 6: Robotic mechanism in vertical position: 1) Stepper motor, 2) Ballscrew, 3) Main sliding block, 4) Wooden base, 5) Supporting structure.

The developed laboratory-scale system is shown in Figure 7. Its design allows for experiments with both the horizontal as well as the vertical coupled ECS configuration. The vertical configuration is shown in Figure 8. The links are made of transparent plexiglass (produced with laser cutting). Each one is composed of two flat pieces assembled together with aluminum spacers (tubes) between them. The developed laboratory-scale system joint's assembly also hosts the electromagnetic brakes and it is installed with low-friction ball bearings. Details of the joints, the joints assembly and the actuation system are shown in Figure 9 and Figure 10, respectively.

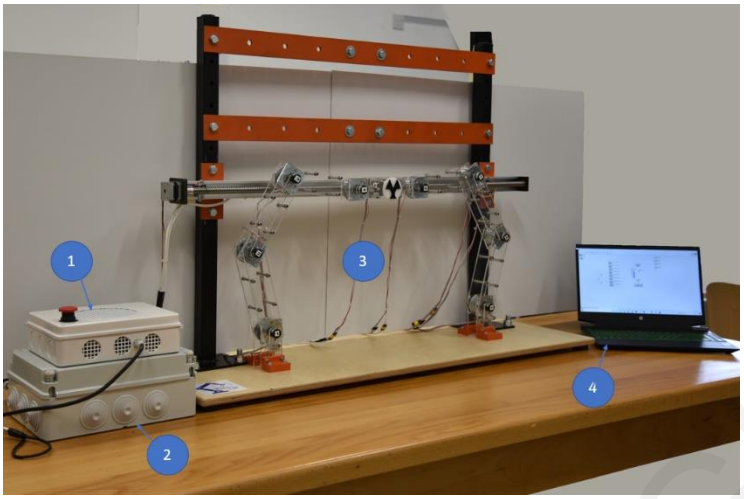

Figure 7: Laboratory setup for horizontal setup: 1) Power supply, 2) Control panel, 3) Robotic mechanism, 4) Graphical user Interface.

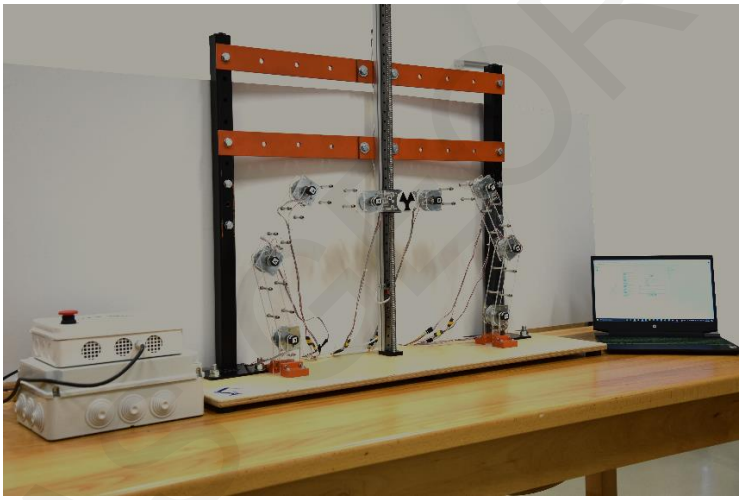

Figure 8: Laboratory setup for vertical setup.

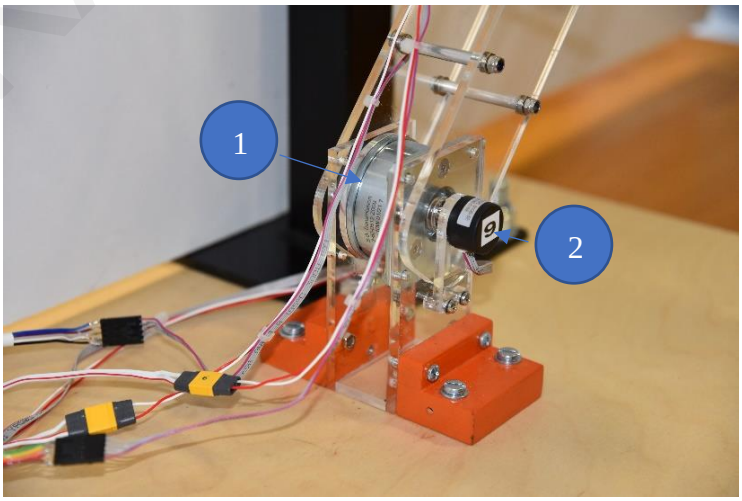

Figure 9: Ground Join: 1) Electromagnetic break, 2) Optical encoder.

The sliding block is connected to the screw slider with four screws to avoid any rotation, as shown in (Figure 10).

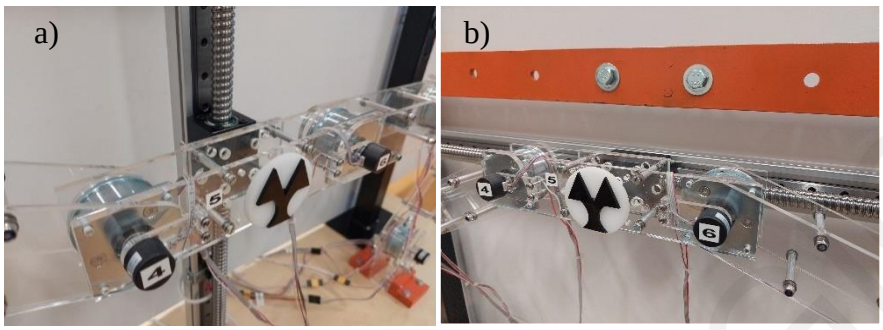

Figure 10: Sliding Block (a) vertical setup, (b) horizontal setup.

Electromagnetic breaks have many applications. Trams and trains use electromagnetic track brakes where the braking element is pressed by magnetic force to the rail. They are distinguished from mechanical track brakes, where the braking element is mechanically pressed on the rail. Electric motors in robotic applications often employ electromagnetic brakes.

Figure 11: Electromagnetic Break (S.G. Transmission 62-0512).

Conventional ‘power- on electromagnetic brakes’ have been utilized in a wide range of motion control applications for decades. More recently applications have tended to focus more on the need to prevent injury in the case of unexpected failure of machines or processes. Whilst there are various fail-safe alternatives including conventional spring applied brakes, there are many advantages to permanent magnet brakes. These brakes are truly fail-safe devices which require no power to give the desired braking action.

For this project, permanent magnetic brakes were used, see Figure 11. These are ‘power off’ devices and are designed so that when the power is removed from the unit, for whatever reason, the magnetic energy of internally mounted permanent magnetic elements to give the required braking effect. The assembly of the e-brake shown in Figure 12. When current is applied through the brakes internal field coil, the magnetic field generated is equal in magnitude and opposite to that of the permanent magnets therefore cancelling each other out. The brake will disengage as the armature plate is pulled off the brake surface by the action of the diaphragm.

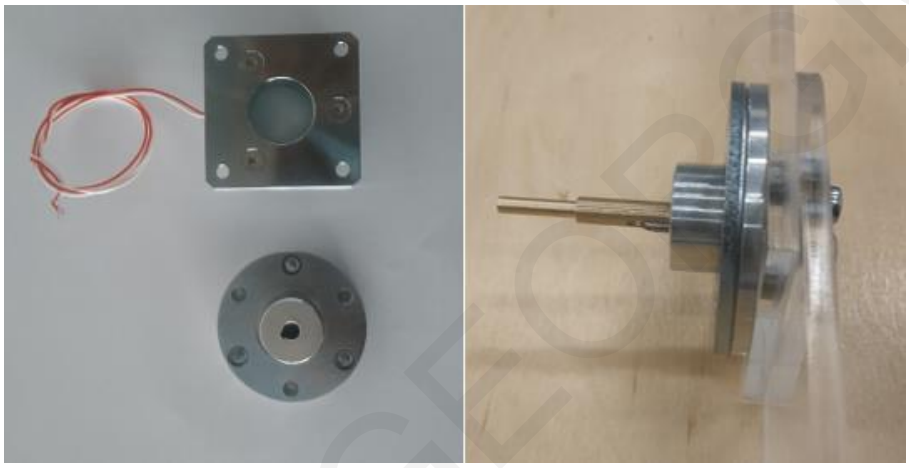

Figure 12: Electromagnetic break assembly,

A stepper motor used to control the angular position of screw slider and the linear movement of the sliding block. Stepper motors can control the angular position of the rotor without a closed feedback loop controller. It is a simple, accurate and open-loop system. A stepper motor is a brushless DC electric motor that divides a full rotation into a number of equal steps. They have multiple coils that are organized in groups called “phases”. The motor will rotate, one step at a time, by energizing each phase in sequence. The stepper motors are the motor of choice for many precision motion control applications. They can achieve very precise positioning and speed control with controlled stepping.

For this project a high torque 42mm Hybrid Stepping Motor was used. This is the bipolar Nema 17 stepper motor with step angle 1.8deg and size 42x42x34mm, as shown in Figure 13. It has 4 wires and each phase draws current 0.4A at 12V, with holding torque 26Ncm.

Figure 13: Bipolar Nema 17 stepper motor,

All the mechanical parts of the robotic mechanism are shown in Figure 14 and Figure 15. Solidworks was used to design the mechanism parts and a complete assembly was generated to match the parts together. An exploded view of the mechanism is presented in Figure 16.

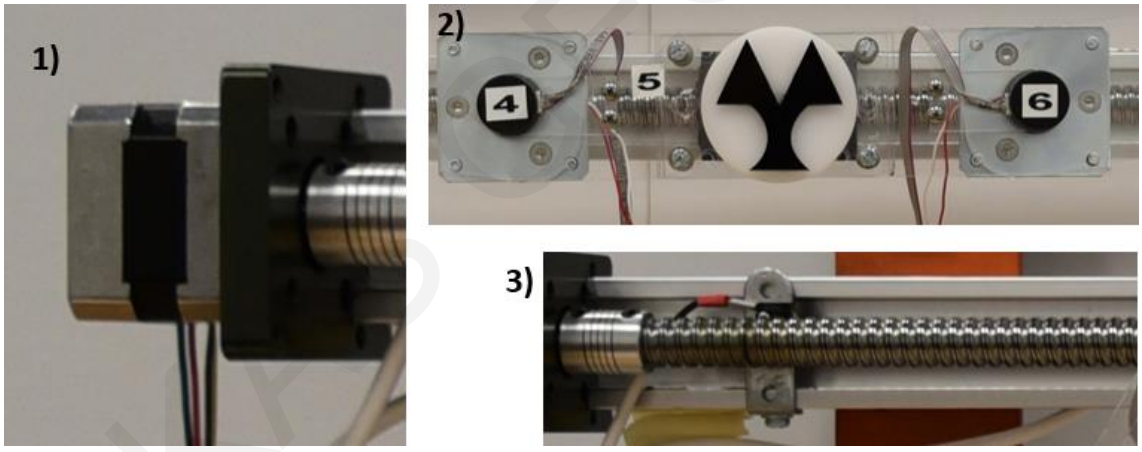

Figure 14: Mechanism components 1) Stepper motor, 2) Sliding block, 3) Ballscrew,

Laser cutting was used to cut the plexiglass. A 2D drawing file was prepared for the laser cutter.

Figure 15: Parts that consists of the mechanism.

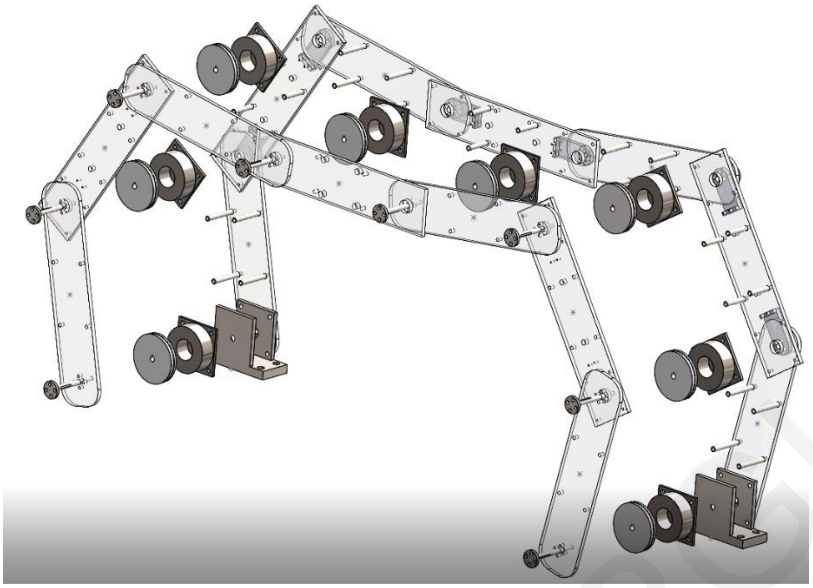

Figure 16: Exploded view of Robotic Mechanism.

2.2 Electrical – Electronics system

The robotic mechanism system communicates with the controller through a computer using the LabVIEW program. Signals from the controller end up in relays. The relay is an electrical switch (Figure 17) that opens and closes an electrical circuit under the control of another electrical circuit as shown in Figure 18.

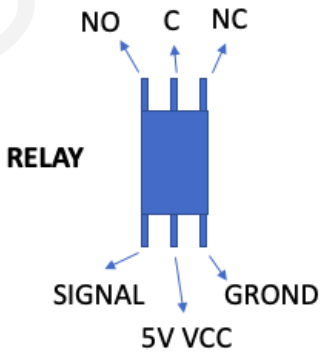

Figure 17: Relay.

For the needs of the mechanism, nine relays have been used. Eight relays control the electromagnetic breaks and another one is used to enable/disable the stepper motor.

An electrical direct current transformer of 5 volts supports the electronic control circuit of eight relays which control the electromagnetic breaks (Figure 19). Another DC transformer of 12 volts powers up the direct circuit of the breaks as shown in Figure 18.

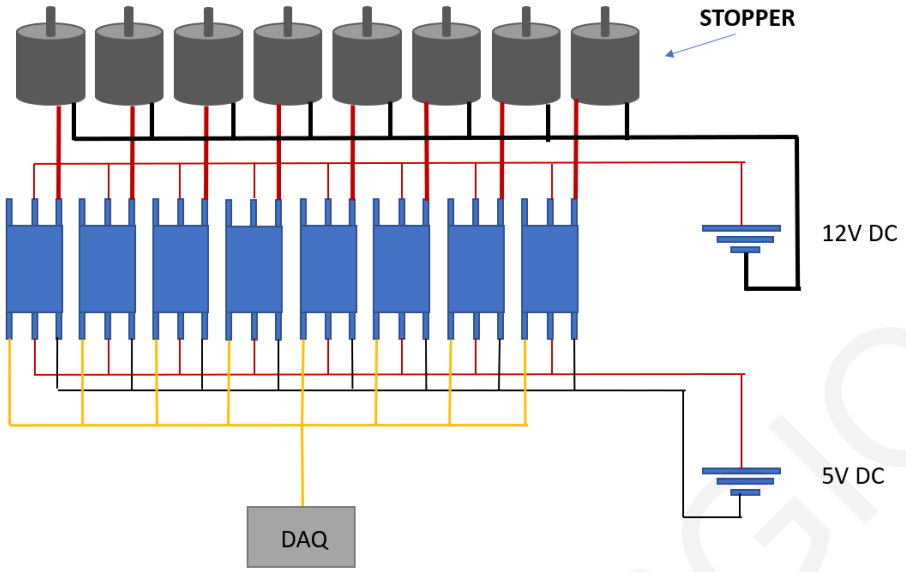

Figure 18: Electromagnetic breaks and relays connection.

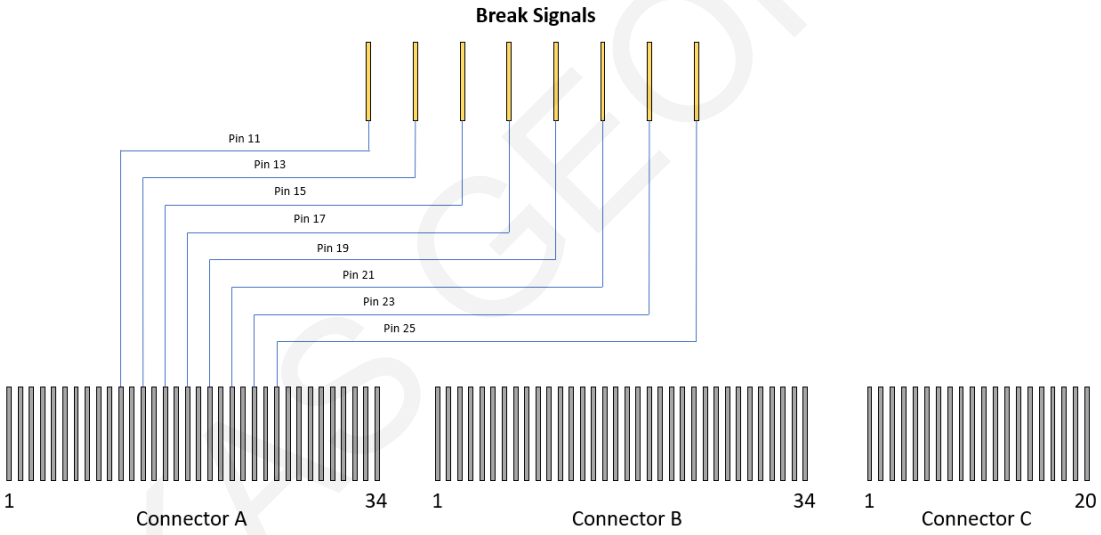

Figure 19: Electromagnetic breaks connection diagram.

Angular position measurements of the links are needed to control the robotic mechanism with accuracy. An optical quadrature encoder (300 counts/rev) is installed on each joint for feedback control purposes. A rotary optical encoder is an electro-mechanical device that converts the angular position or motion of a shaft to analog or digital output signals. For this application was used the optical encoder HKT22, as shown in Figure 20. This optical encoder can be attached to a 4mm rear shaft. It provides 300 counts (full quadrature cycles) per rotation. Figure 20 shows parts of the optical encoder and Figure 21 presents analytically the wiring connections with the controller.

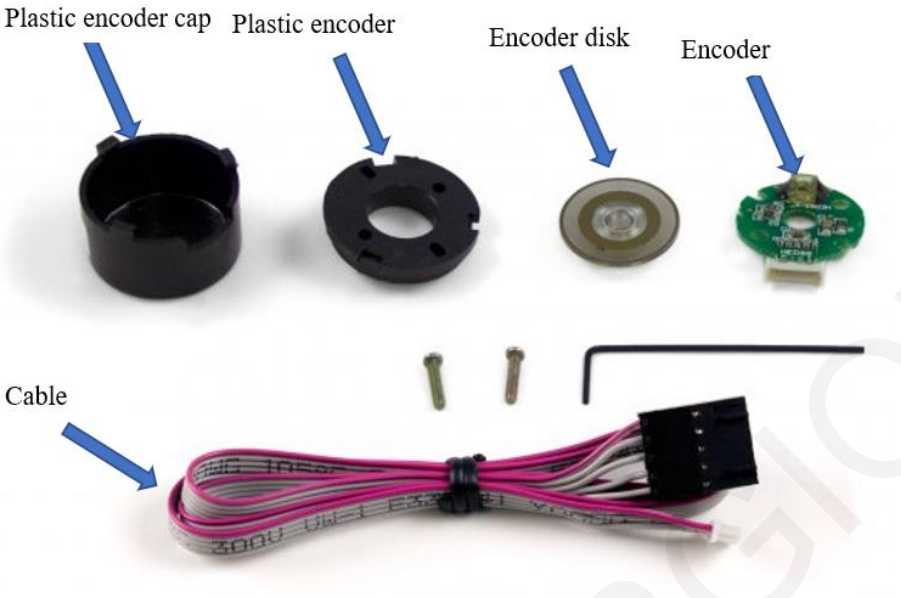

Figure 20: Optical Encoder HKT22 Parts.

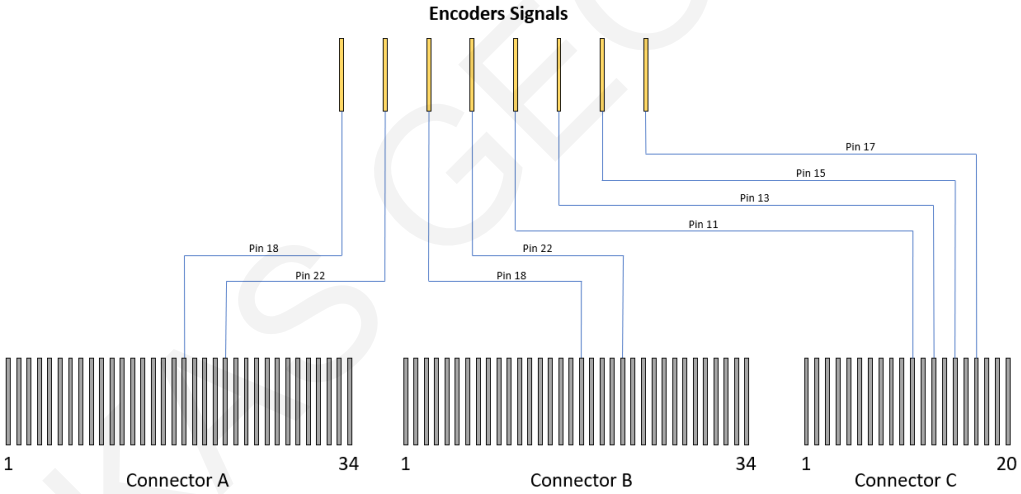

Figure 21: Optical encoders connection diagram.

The Optical encoders are installed on the joins to calculate the relative movement of the links. The encoder disk connects to the axis which is connected with the outer link. The encoder board with the plastic case connects to the inner link to capture the relative movement, as shown in Figure 22.

Figure 22: Optical Encoder installation.

The signal cables of the optical encoders are connected with VGA and pin connectors, as shown in Figure 23a,b.

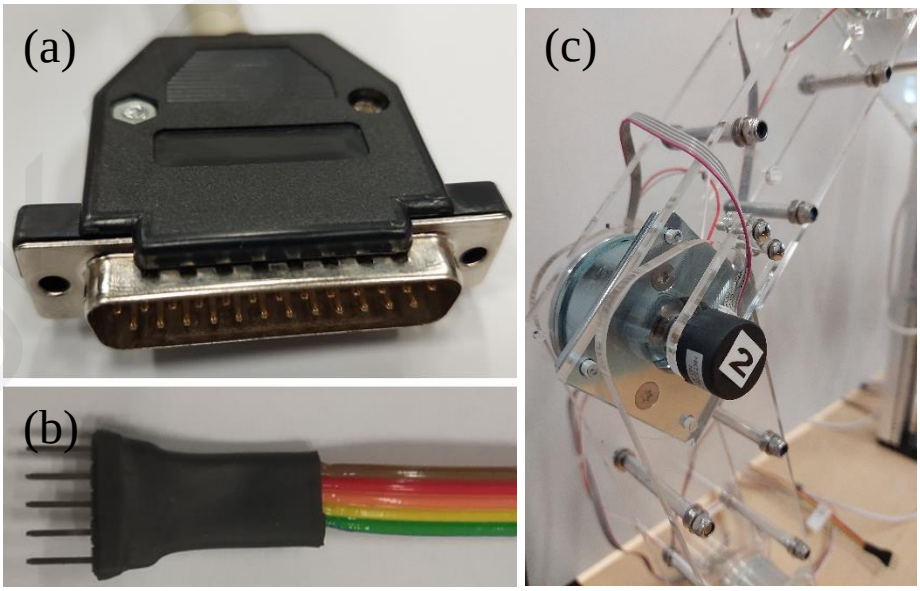

Figure 23: VGA and Pin connector of optical encoder.

A stepper motor driver was used to control the precise movement of stepper motor. For the purpose of this applications a TB6600 driver was used. The TB6600 driver is an easy-to-use professional stepper motor driver, which could control a two-phase stepping motor. It is compatible with LabVIEW DAG's and other microcontrollers that can output a 5V digital pulse signal. The TB6600 stepper motor driver has a wide range power input, 9~42VDC power supply. It is able to output 4A peak current, which is enough for most of the stepper motors. This driver is shown in Figure 24 and the characteristics in Appendix II.

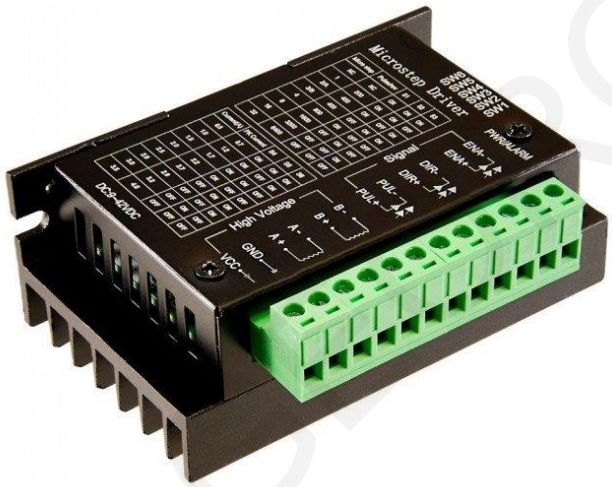

Figure 24: TB6600 stepper motor driver.

For safety purposes and also to protect the components from dust and moisture, the transformers, the electronic circuits of the relays and the MyRIO control card, were placed in two insulating boxes. These boxes are not electrically penetrated, creating a safe environment for their users, offering them protection against electric shock.

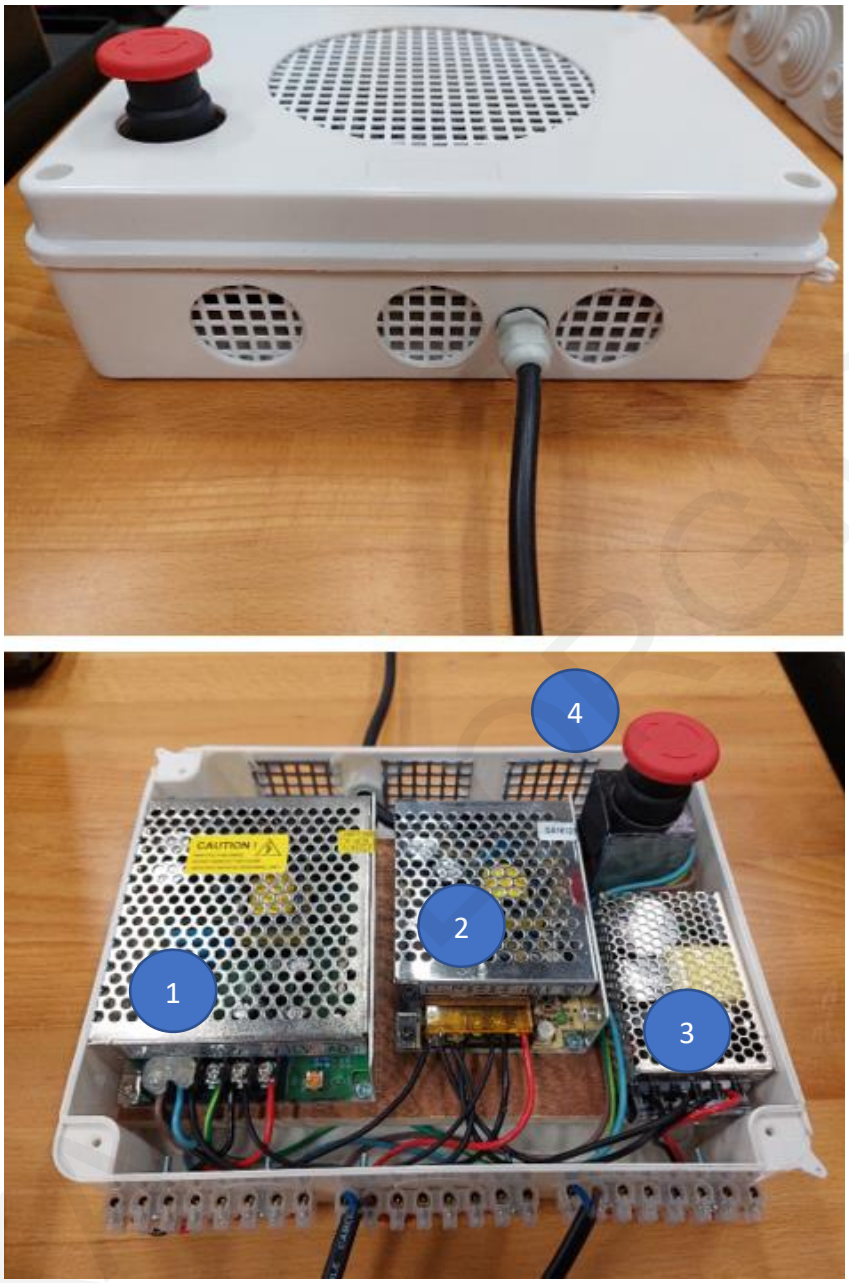

Figure 25: Insulating transformer box with emergency switch: 1) 24V transformer, 2) 12V transformer, 3) 5V transformer, 4) Emergency switch.

In the first insulating box, as shown in Figure 25 a piece of wood was placed at the bottom, where the three transformers were fixed with screws. Three sets of connectors were attached to the box corresponding to each transformer. Each set has a negative and a positive charge, distinguishing it by the color of the cables. Red represents the positive and black the negative. An emergency button was installed to cut off the power in case of emergency. Also, vents for air circulation were added to allow colling of the transformers.

An emergency stop switch is a safety mechanism used to shut off the mechanism in an emergency, when it cannot be shut down in the usual manner. The purpose of an emergency push button is to stop the mechanism quickly when there is a risk of injury or the robotic operation requires immediate stopping.

The design and construction of these boxes is a very important part of the work and a lot of time was devoted to their construction. All cables that go in and out of the box are secured with cable glands (see Figure 26) ensuring the insulation of the holes and the stability of the cables. Cable glands play an important role in cable management.

Figure 26: Cable Glands.

The second insulating box contains the electronic parts. As with the transformer box, all the components were installed on a wooden base, see Figure 27.

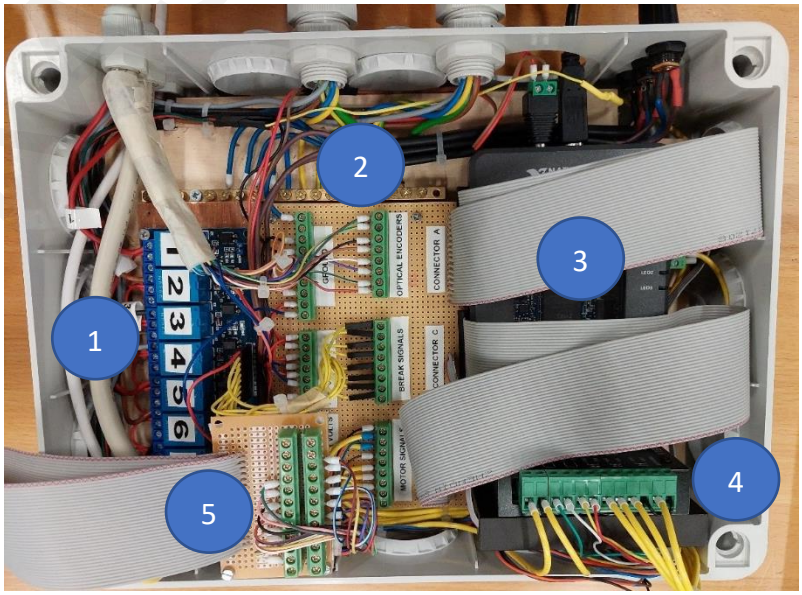

Figure 27: Electronic Insulation box 1) Relays, 2) Main electronic board, 3) MyRIO, 4) Stepper motor driver, 5) External electronic board.

Cable glands were attached to the back of the box to secure the cables, as shown in Figure 28. The cable gland compresses a seal into the round cable. It stops ingress of particles or water which could cause damage to the electronic devices.

Figure 28: Inputs and outputs for power and signal of the mechanism.

Proper installation of the power cables is a prerequisite when starting the mechanism. First the 5V power cable is installed to start the control systems, then the 12V cable is installed which activates the electromagnetic brakes and finally the 24V cable to supply the screw slider, as shown in Figure 29. In case they are placed in a different order, the control system will not work properly, causing irregular operation of the mechanism.

Figure 29: Power inputs.

All the signal and power cables required for the operation of the robotic mechanism must be disconnected in order to transport the mechanism. Before the power is plugged all the connections must be checked.

2.3 Control hardware and software

The software used to program the device is National Instruments LabVIEW (Laboratory Virtual Instruments Engineering Workbench). LabVIEW is a visual programming language platform for system design. This graphical programming language is also called ‘G’. It first appeared on the Apple Macintosh in 1986. It is used to receive data from external sensors, to control external instruments and for industrial automation in a variety of software.

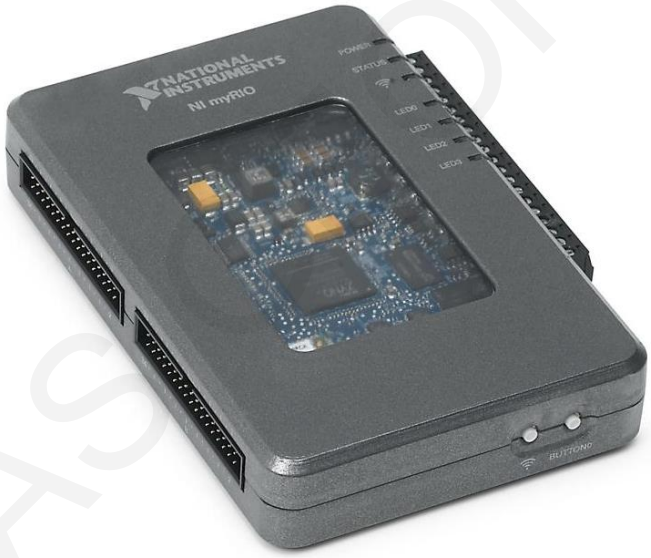

Figure 30: NI myRIO.

MyRIO is the controller which connects the graphical interface on the computer with the robotic mechanism. The controller, as shown in Figure 30 Student Embedded Device features I/O on both sides of the device in the form of MXP and MSP connectors. It includes analog inputs and outputs, digital I/O lines, LEDs, a push button, an onboard accelerometer, a Xilinx FPGA, and a dual-core ARM Cortex-A9 processor. Some models also include WiFi support. You can program myRIO Student Embedded Device with LabVIEW or C. A schematic of the output pins of the controller shows in Figure 31.

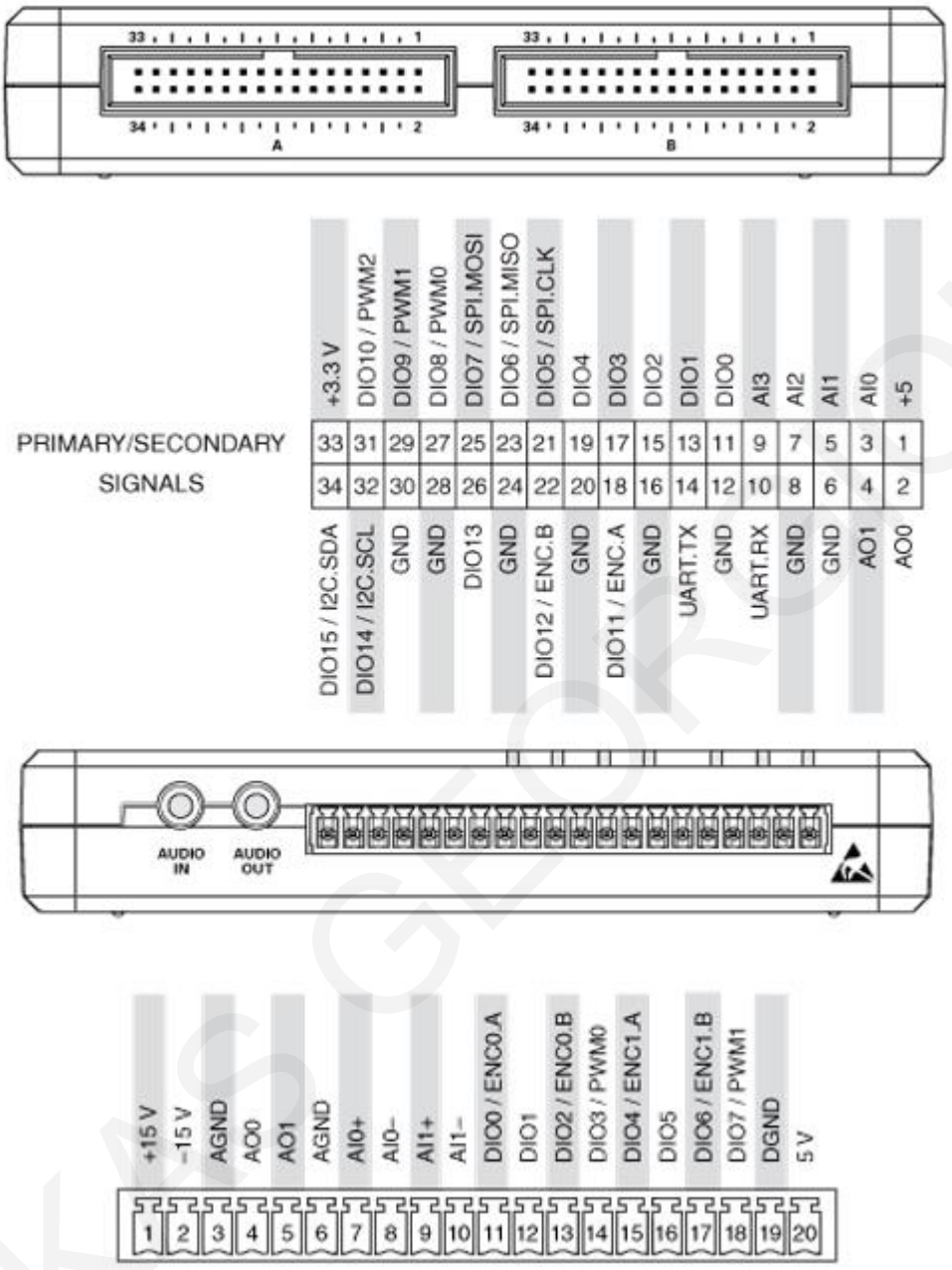

Figure 31: MyRIO I/O Connectors.

The code in LabVIEW software was written graphically, as shown in Figure 32. Several data acquisitions (DAQ) were used for input and output (I/O) signals. The DAQ Assistant is a graphical interface for configuring measurement tasks and channels and for customizing timing, triggering, and scales. Seven analog inputs and nine digital outputs were used to operate the n-bars. Nine digital outputs and seven analog inputs were generated to control the digital outputs and analog inputs of the device.

The tables below show the control and power cable connections from MyRIO.

Table 1 shows the stepper motor and driver connections. Pin 27 from connector B generate the pulse signal for the stepper motor that moves the ballscrew. Connector A controls the motor power and direction. The direction (clockwise/counterclockwise) from pin 27 and the power (enable/disable) from pin 29. Each pin number on Table 2 corresponds to each one of the 8 e-breaks of connector A.

Table 3 and Table 4 represent the wire connection of VGA-A and VGA-B.

Table 1: Stepper motor and drive connections.

STEPPER MOTOR AND DRIVER		
PIN NAME	PIN NUMBER	CONNECTORS
PULES SIGNAL	27	Connector B
DIRECTION	27	Connector A
ENABLE/DISABLE	29	Connector A

Table 2: Connection of the Breaks.

BREAKS		
PIN NAME	PIN NUMBER	CONNECTORS
BREAK 1	11	Connector A
BREAK 2	13	
BREAK 3	15	
BREAK 4	17	
BREAK 5	19	
BREAK 6	21	
BREAK 7	23	
BREAK 8	25	

Table 3: VGA - A connections.

VGA - A							
Male		Female			PIN NUMBER	PHASE	CONNECTORS
1	-	1	-	-			
2	-	2	-	-			
3	-	3	-	-			
4	white	4	blue	0V			
5	white-blue	5	purple	NC	Not connected		
6	yellow -blue	6	γρκιζο	CHB	22	Phase B	Connector A
7	orange	7	white	5V			
8	red-blue	8	black	CHA	18	Phase A	Connector A
9	yellow-orange	9	blue	0V			
10	yellow	10	purple	NC	Not connected		
11	white-red	11	grey	CHB	22	Phase B	Connector B
12	black-blue	12	white	5V			
13	purple	13	black	CHA	18	Phase A	Connector B
14	-	14	-	-	Not connected		
15	-	15	-	-			
16	blue-orange	16	brown	0V			
17	blue-grey	17	red	NC	Not connected		
18	black	18	orange	CHB	13	Phase B	Connector C
19	red	19	yellow	5V			
20	brown	20	green	CHA	11	Phase A	Connector C
21	pink	21	brown	0V			
22	brown-red	22	red	NC	Not connected		
23	brown-green	23	orange	CHB	17	Phase B	Connector C
24	blue	24	yellow	5V			
25	yellow-green	25	green	CHA	15	Phase A	Connector C

Table 4: VGA - B connections.

VGA - B					
Male		Female			
1	-	1	-	-	Not connected
2	-	2	-	-	
3	-	3	-	-	
4	white	4	green	CHA	
5	white-blue	5	yellow	5V	
6	yellow -blue	6	orange	CHB	
7	orange	7	red	NC	
8	red-blue	8	brown	0V	
9	yellow-orange	9	green	CHA	
10	yellow	10	yellow	5V	
11	white-red	11	orange	CHB	
12	black-blue	12	red	NC	
13	purple	13	brown	0V	
14	-	14	-	-	
15	-	15	-	-	
16	blue-orange	16	black	CHA	
17	blue-grey	17	white	5V	
18	black	18	grey	CHB	
19	red	19	purple	NC	
20	brown	20	blue	0V	
21	pink	21	black	CHA	
22	brown-red	22	white	5V	
23	brown-green	23	grey	CHB	
24	blue	24	purple	NC	
25	yellow-green	25	blue	0V	

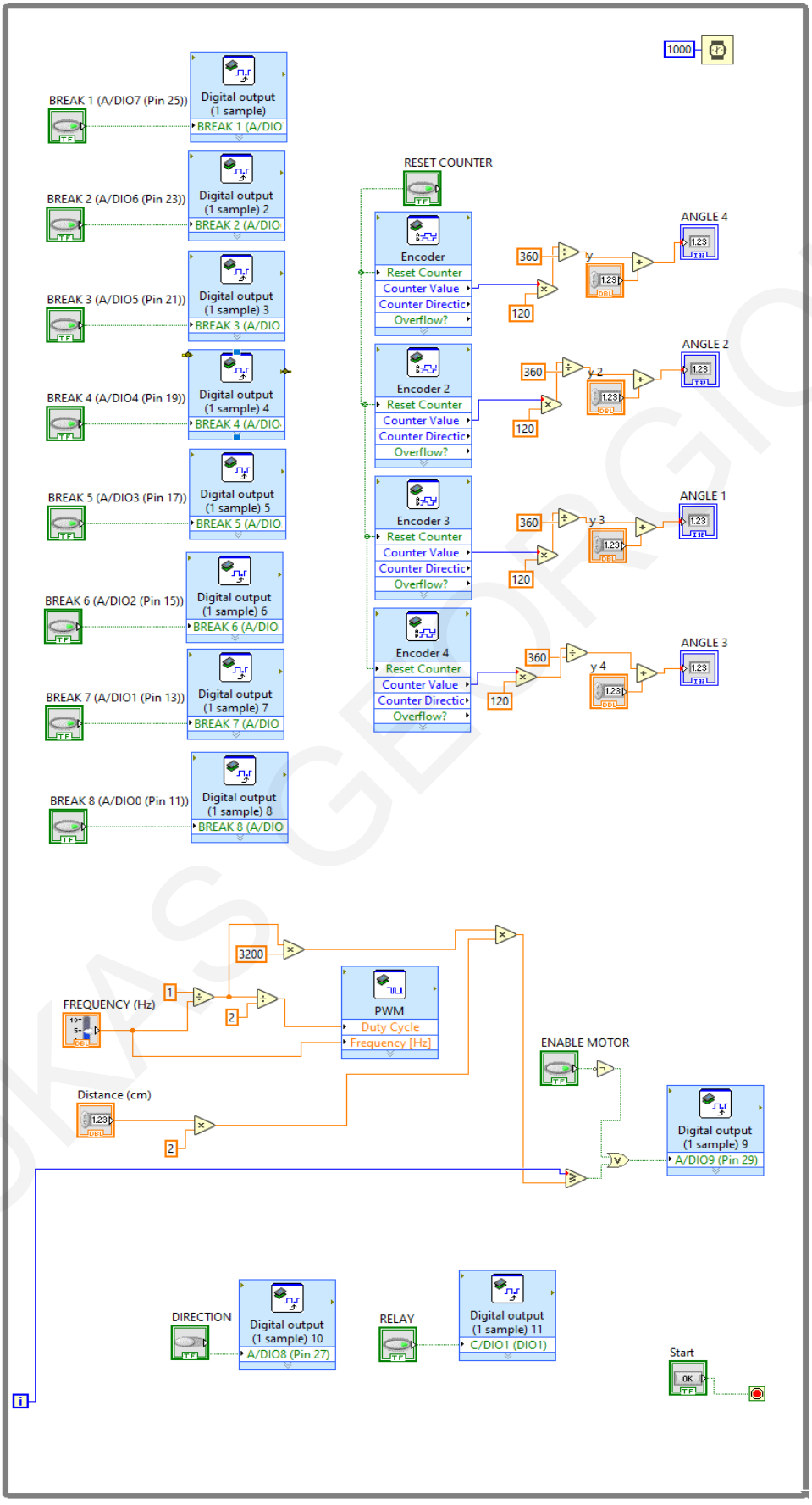

Figure 32: Block diagram – Code.

Nine different DAQs were used for the nine digital signals to control the eight breaks and the relay for the activation of the stepper motor driver, while one analog DAQ was used to control the stepper motor frequency. Bush buttons connected to control the digital signals and an analog slider to control the frequency. All together are placed in a while loop. The while loop provides continuous program operation until the stop button is activated.

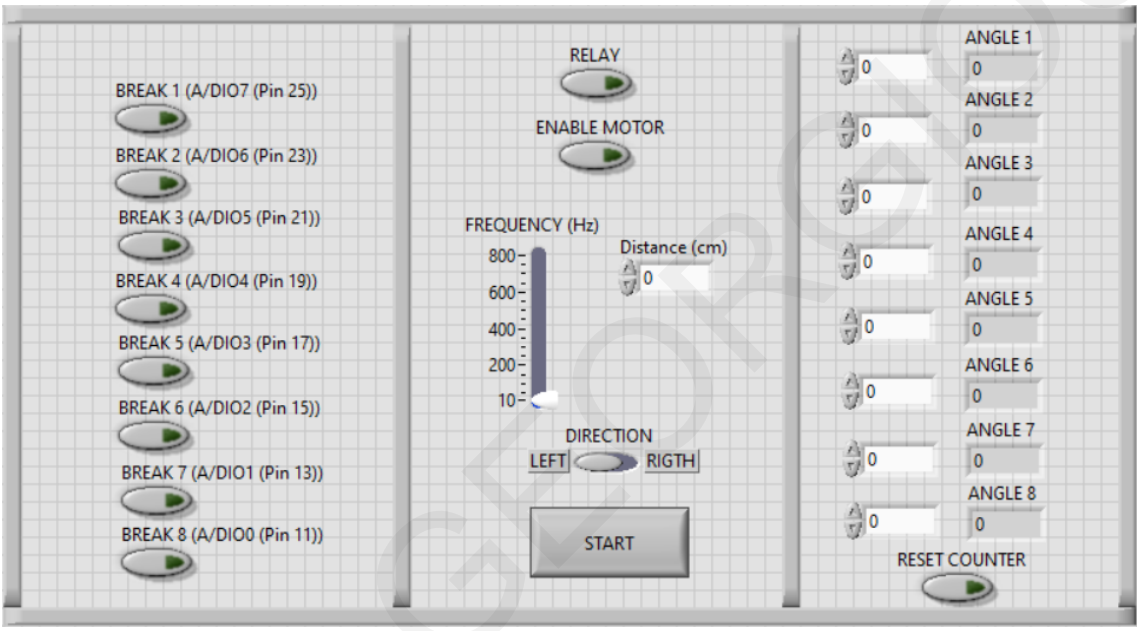

Figure 33: Front panel - User interface.

Figure 33 shows the interface of the robotic mechanism control program. The interface is divided into 3 main parts: Breaks, Slider and Degrees. The Break part consists of eight buttons which control the electromagnetic brakes of the mechanism. E-brakes are always normally locked for safety reasons. By activating the buttons 1 to 8 they can be unlocked, leaving the links free to move. The second section consists of four buttons: Relay, Enable motor, Distance and Start, that control the movement (right - left) of the screw driver. In the third section, there is an array type table in which during the operation of the program the rotations of the joints 1 to 8 are presented.

Table 5 shows the functionalities, of each button.

Table 5: Interface buttons description,

Button name	Functions
BREAK 1	Enable break 1
BREAK 2	Enable break 2
BREAK 3	Enable break 3
BREAK 4	Enable break 4
BREAK 5	Enable break 5
BREAK 6	Enable break 6
BREAK 7	Enable break 7
BREAK 8	Enable break 8
RELAY	Power up stepper motor
ENABLE MOTOR	Enable stepper motor driver
DIRECTION	Select diraction of the main sliding block
START	Enable stepper motor
RESET COUNTER	Reset optical encoders mesurments
ANGLE 1	Relative angle 1 in degrees
ANGLE 2	Relative angle 2 in degrees
ANGLE 3	Relative angle 3 in degrees
ANGLE 4	Relative angle 4 in degrees
ANGLE 5	Relative angle 5 in degrees
ANGLE 6	Relative angle 6 in degrees
ANGLE 7	Relative angle 7 in degrees
ANGLE 8	Relative angle 8 in degrees

Chapter 3

3 SIMULATION AND EXPERIMENTAL STUDIES

3.1 Motion Planning

A reconfiguration between an initial and a final configuration can be realized using alternative control sequences. Motion planning is choosing convenient sequences that respect joint motion constraints while avoiding singular configurations and collisions. Many different possible reconfiguration sequences exist in most cases, and an optimization process can be used to choose the best one. Energy usage, actuation effort, and reconfiguration times are all possible optimization criteria.

The proposed reconfiguration approach, which is similar in concept to all other coupled mechanisms, was demonstrated using simulations and experimental studies using the coupled ECS concept (horizontal version). During both the simulation model and the laboratory setup, the slider is moved by the actuator along a horizontal rail that is installed at a height (H) of 32.75 cm above the ground. Three serially connected links are attached to either side of the slider block, with the other end being pin-connected to the ground. The links and the slider block have a joint-to-joint distance of 19.5. The distance between the two ground supports (L) is 70.5 cm, as shown in Figure 34. All rotational joints (including the ground ones) are equipped with brakes and joint-position measurements are available.

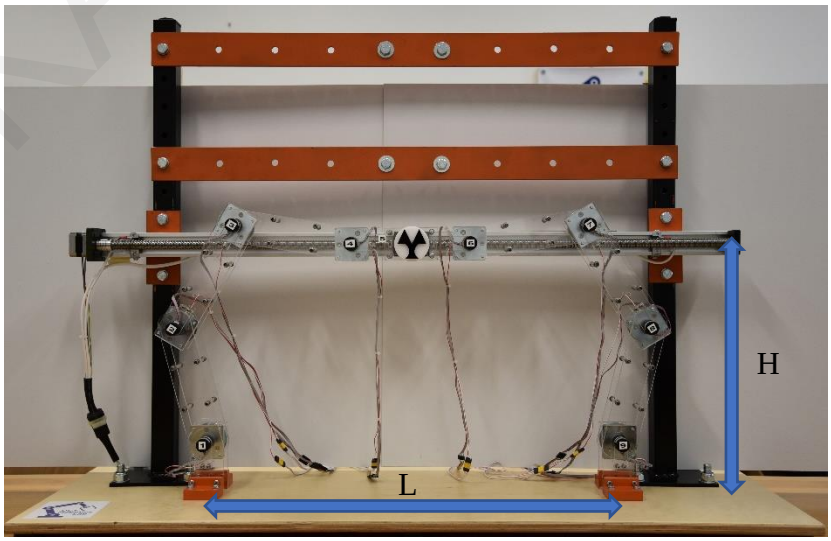

Figure 34: General dimensions of robotic mechanism.

(i)

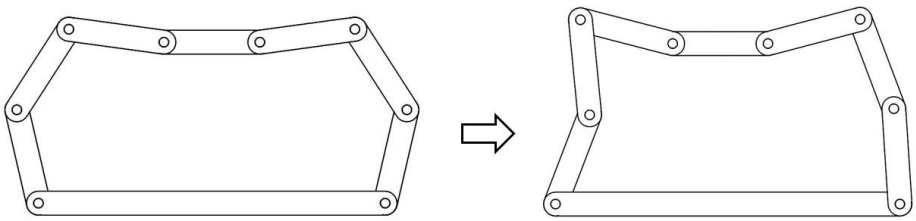

(a)

	Joint 1	Joint 2	Joint 3	Joint 4	Joint 5	Joint 6	Joint 7	Joint 8	Joint 9
Step 1	△	⊙	⊗	⊙	▭	⊙	⊙	⊙	△
Step 2	△	⊙	⊙	⊙	▭	⊙	⊗	⊙	△
Step 3	△	⊙	⊗	⊙	▭	⊙	⊗	⊙	△

(b)

	Joint 1	Joint 2	Joint 3	Joint 4	Joint 5	Joint 6	Joint 7	Joint 8	Joint 9
Step 1	△	⊙	⊗	⊙	▭	⊙	⊙	⊗	△
Step 2	△	⊗	⊙	⊙	▭	⊙	⊗	⊙	△
Step 3	△	⊙	⊗	⊙	▭	⊙	⊗	⊙	△

(c)

(ii)

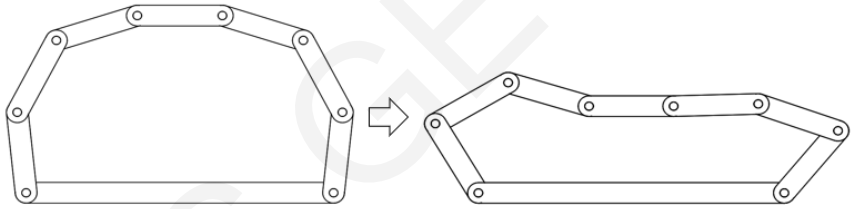

(a)

	Joint 1	Joint 2	Joint 3	Joint 4	Joint 5	Joint 6	Joint 7	Joint 8	Joint 9
Step 1	△	⊙	⊙	⊗	▭	⊗	⊙	⊙	△
Step 2	△	⊗	⊙	⊙	▭	⊗	⊙	⊙	△
Step 3	△	⊗	⊙	⊙	▭	⊙	⊗	⊙	△

(b)

	Joint 1	Joint 2	Joint 3	Joint 4	Joint 5	Joint 6	Joint 7	Joint 8	Joint 9
Step 1	△	⊙	⊗	⊙	▭	⊗	⊙	⊙	△
Step 2	△	⊗	⊙	⊙	▭	⊗	⊙	⊙	△
Step 3	△	⊗	⊙	⊙	▭	⊙	⊙	⊗	△

(c)

Figure 35: Scheduling tables that correspond to two feasible control sequences for the required shape adjustment. (a) Initial and target configurations for the simulation and experimental study. (b) Sequence I; (c) Sequence II (⊗: locked joint, ⊙: unlocked joint, △: pivoted–to–the–ground joint, symbols in red color represent the currently adjusted joints). (i) Horizontal motion, (ii) Vertical motion.

Both simulations and experiments are based on the same system and run the same control sequences (Sequence I and Sequence II), as shown in Figure 35. The Figure 35a illustrates the initial and final configurations of the structure. In both sequences, these are described by the vectors of internal joint angles (clockwise, starting on the left ground joint):

Horizontal motion

$\boldsymbol{\theta_i}$ = [103.01, 134.18, 115.04, 187.77, 187.77, 115.04, 134.18, 103.01] degrees
$\boldsymbol{\theta_f}$ = [69, 206.57, 70, 194.44, 194.7, 96, 163, 86.3] degrees

Vertical motion

$\boldsymbol{\theta_i}$ = [95.98, 146.63, 135.22, 162.17, 162.17, 135.22, 146.63, 95.98] degrees
$\boldsymbol{\theta_f}$ = [120.56, 90.12, 132.28, 197.03, 181.57, 158.96, 70.06, 129.40] degrees

3.2 Simulation Study

A convenience of simulation studies is the ability to understand the behavior of the mechanism before you make it real. Good understanding leads to more appropriate solutions and make the final product more efficient and safer.

For the needs of this Master's thesis, simulation studies and motion analysis have been prepared. Motion studies ran on Solidworks and include all 95 physical components and construction details of the system (links, brakes, encoders, etc.). Horizontal and vertical position of the screw slider were prepared and simulated to examine their behavior (illustrated in Figure 36 and Figure 37). Perfect brake actions with zero backlash and elasticity are assumed along with perfectly rigid links. Programing of motion was held in tasks. Four intermediate positions are reached in order to complete each motion.

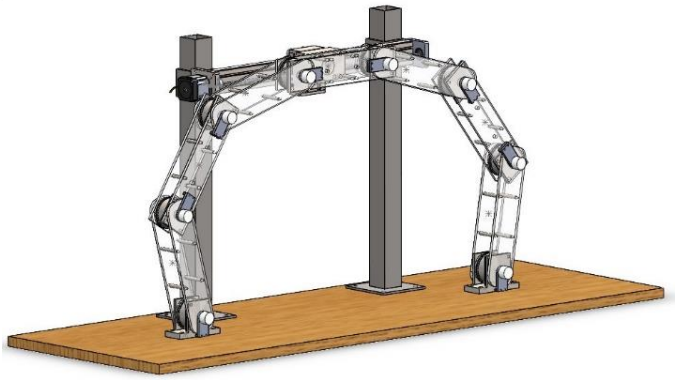

Figure 36: 3D model of the planar closed-chain mechanism for the motion studies (Horizontal motion actuator).

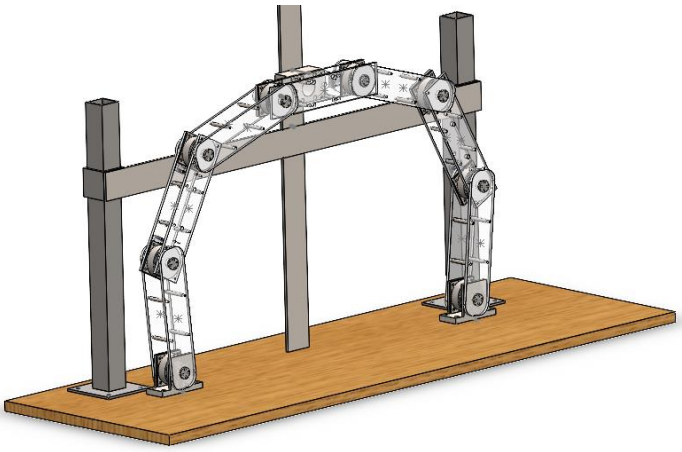

Figure 37: 3D model of the planar closed-chain mechanism for the motion studies (Vertical motion actuator).

The simulated reconfiguration of the system in all intermediate positions during reconfiguration is shown in Figure 38 and Figure 39, and for the two horizontal and vertical control sequences, respectively.

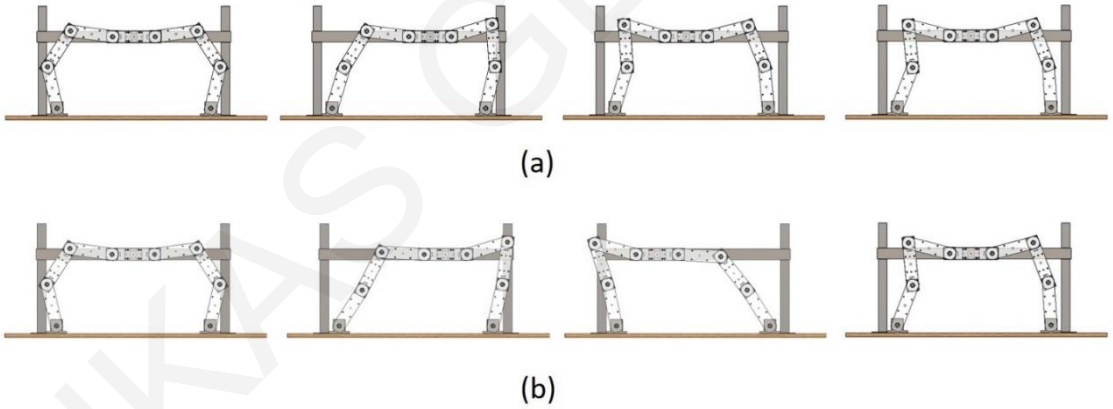

Figure 38: Intermediate positions for the simulated reconfigurations between the initial and target positions. (a) Sequence I; (b) Sequence II. (Horizontal motion).

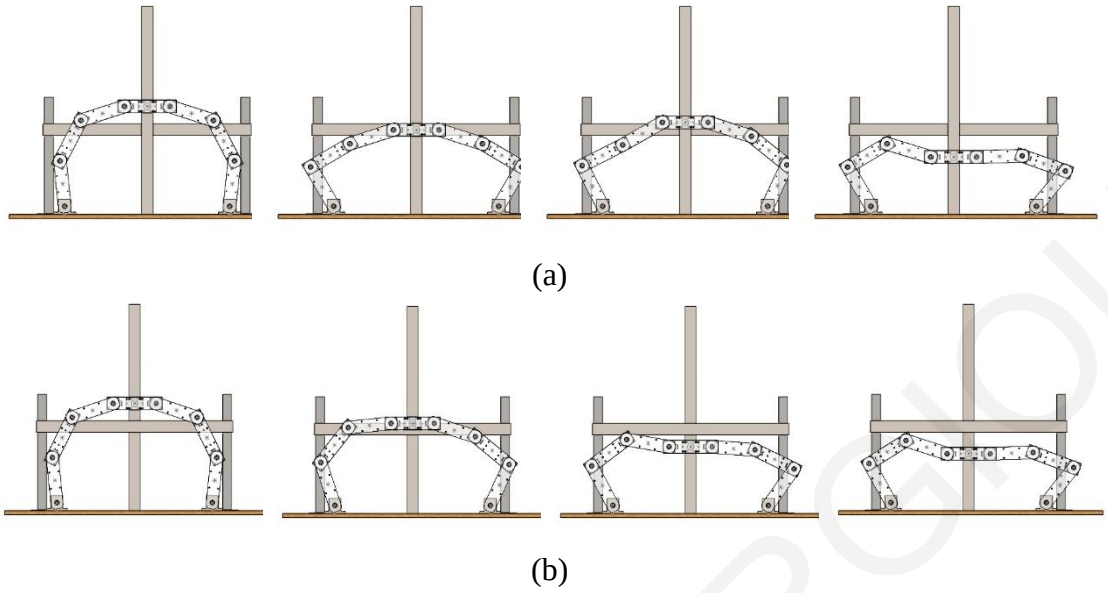

(a)

(b)

Figure 39: Intermediate positions for the simulated reconfigurations between the initial and target positions. (a) Sequence I; (b) Sequence II. (Vertical motion).

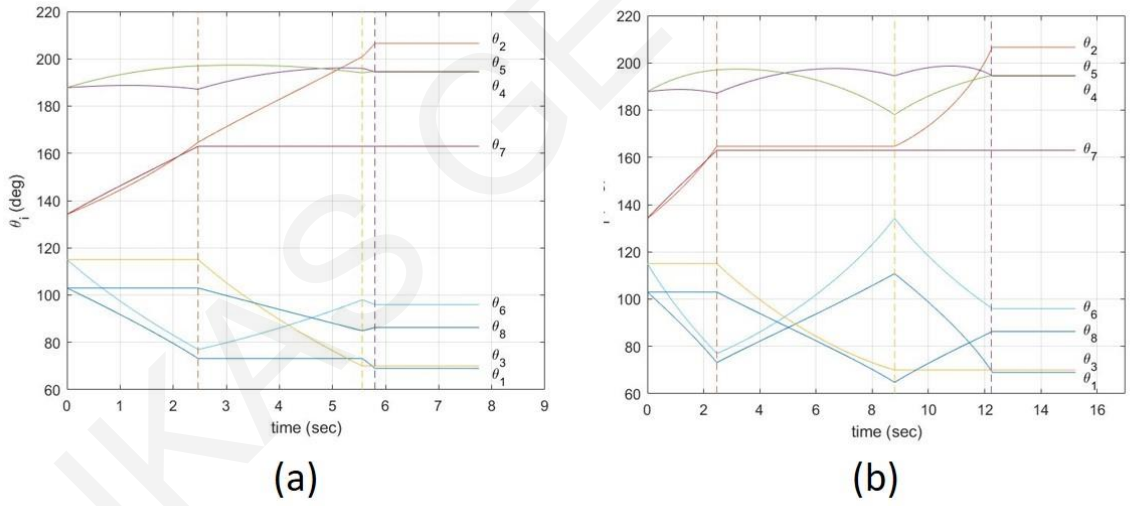

Figure 40: Time histories for the joint motion during reconfiguration between the initial and the final configuration. (a) Sequence I; (b) Sequence II. The vertical zones correspond to the individual time steps. In both sequences, the adjustment of θ7 is completed in the first step, θ3 is adjusted as part of the second step, and the rest of the joint angles are adjusted simultaneously in the last step (Horizontal motion).

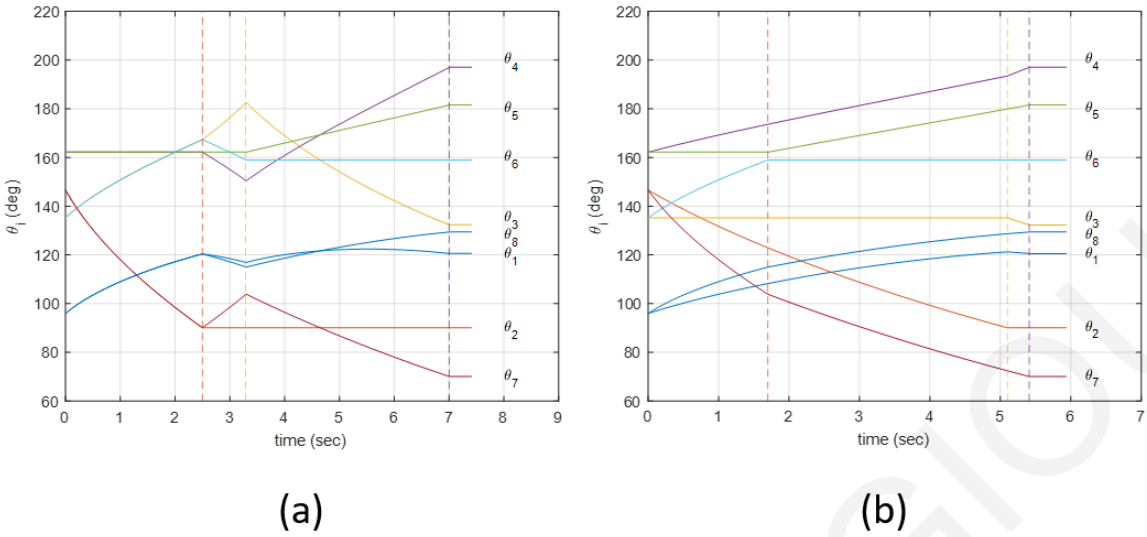

Figure 41: Time histories for the joint motion during reconfiguration between the initial and the final configuration. (a) Sequence I; (b) Sequence II. The vertical zones correspond to the individual time steps (Vertical motion).

Table 6: Reconfiguration times (in seconds) for the two examined sequences. (a) horizontal motion; (b) vertical motion

Sequence	Step 1	Step 2	Step 3	Total
I	2.47	3.09	0.24	5.8
II	2.47	6.32	3.48	12.27

(a)

Sequence	Step 1	Step 2	Step 3	Total
I	2.50	0.8	3.71	7.01
II	1.70	3.40	0.31	5.41

(b)

The time histories of the joint angles during the reconfiguration (for both sequences and setups) are shown in Figure 40 and Figure 41, using a fixed linear speed for the slider (20 mm/s). The results clearly demonstrate the control philosophy: in each step a different effective mechanism is defined and a corresponding joint angle is adjusted, which remains locked in the next steps. The same procedure is repeated until the reconfiguration is fully completed. The times required to complete each reconfiguration step were recorded in Table 6. Interestingly, the times differ considerably between the two sequences. This suggests that the overall reconfiguration time provides a reasonable criterion for comparing alternative control sequences in order to select the most suitable

one. For a fixed slider velocity this also translates to minimum required actuator motions. In horizontal actuator motion, Sequence I provides a clear advantage in that respect and in the vertical motion the total time of Sequence II is slightly greater than Sequence I. Other criteria for the evaluation of control sequences may refer to the work done by the actuators during reconfiguration and the maximum required brake torques.

3.3 Experimental Study

The experimental study took place after the simulation study to confirm the results. The laboratory-scale system was developed and assembled at the robotic laboratory of University of Cyprus (UCY Robotics Lab) with respect to the simulated mechanism. Its design allows for experiments with both the horizontal as well as the vertical coupled ECS configuration.

The same reconfiguration sequences as before were also used for the experiments, and the intermediate reconfiguration steps are depicted in Figure 42. The similarity with the simulation results in Figure 38 and Figure 39 is obvious, showing that even the small friction at the joints (not included in the model) does not affect the final configuration.

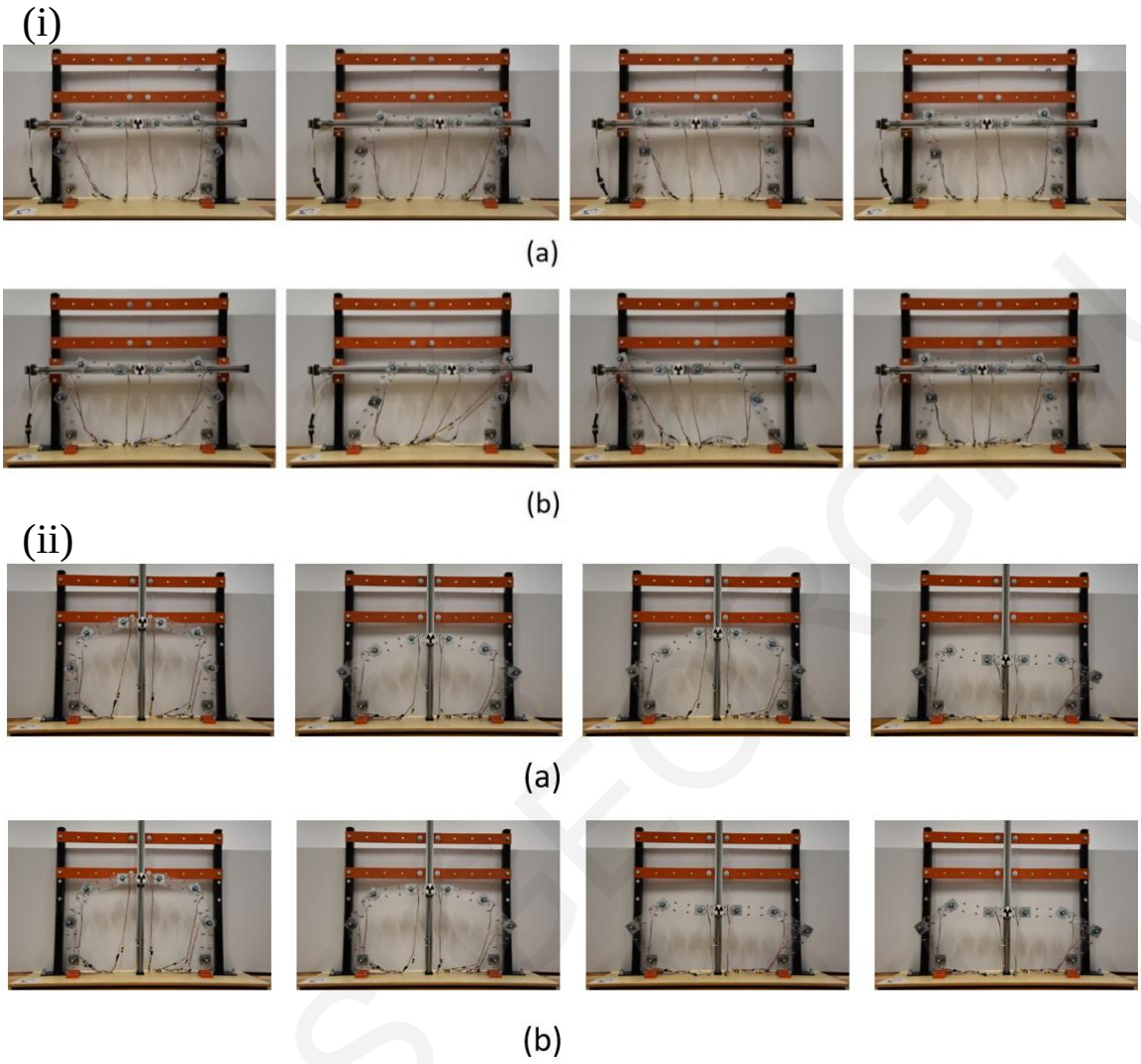

Figure 42: Reconfiguration experiments using the coupled ECS method between the selected initial and final configuration. (i) Horizontal motion, (ii) Vertical motion, (a) Sequence I, (b) Sequence II.

Chapter 4

4 DYNAMICS MODELING

In order to create dynamic system models the bond graph methodology [9] has been used in this project. This type of methodology is applied to identify the system's prominent dynamic features during reconfiguration and reduce the model's complexity that will later aid the controller design [10]. Moreover, for the bond graph user interface and simulation software the 20SIM has been chosen. This program uses modular element libraries to combine bond graphs and block diagrams [11]. Then the bond graph is automatically converted into an equation model by 20SIM that will numerically integrate systems of equations.

Figure 43 illustrates the development of the left side of the CECS mechanism using the bond graph model. The graph shows the two links of the model. The first joint of Link 1 is pivoting to the ground and its second link uses Link 2 to connect to the slider. The R elements represent the bearing friction if the brakes are not enabled. The multiport model of the two links is represented by the bond graph in Figure 44. The graph shows the I and MTF junctions elements that represent all inertial effects in both rotation and translation and the kinematics and gravitational forces respectively. Moreover, the slider is connected to the motor with a ballscrew create a model that includes its mass and friction. When the motor drives the ballscrew inertial and dissipative effects are created from the electrical and mechanical parts. As the major powers that have effects on the mechanism are shown on the bond graph it is easy to investigate design improvements for greater performance.

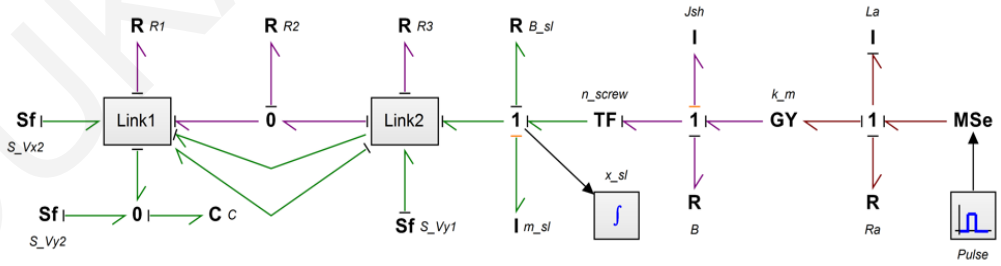

Figure 43: Bond graph model of CECS mechanism with the driving motor/ballscrew.

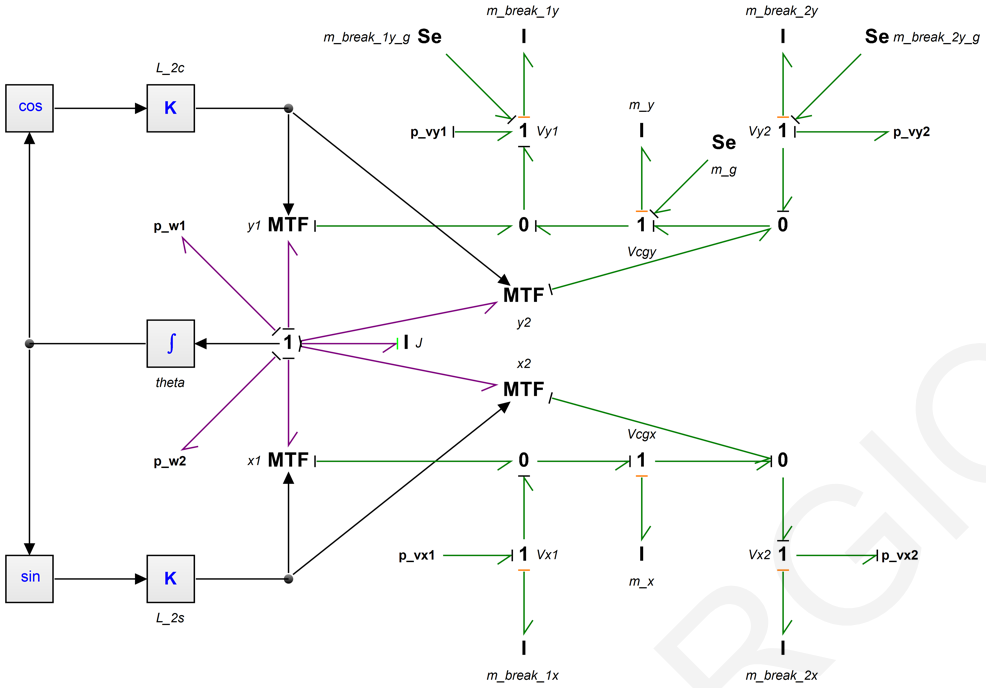

Figure 44: Bond graph model of a link with 2 joints.

The links of the mechanism have three degrees of freedom (X,Y,Θ). Plane motion study without fix axis was used to model the links. A free body diagram was develop, as shown in Figure 45 and the four equations of the linear velocities were calculated.

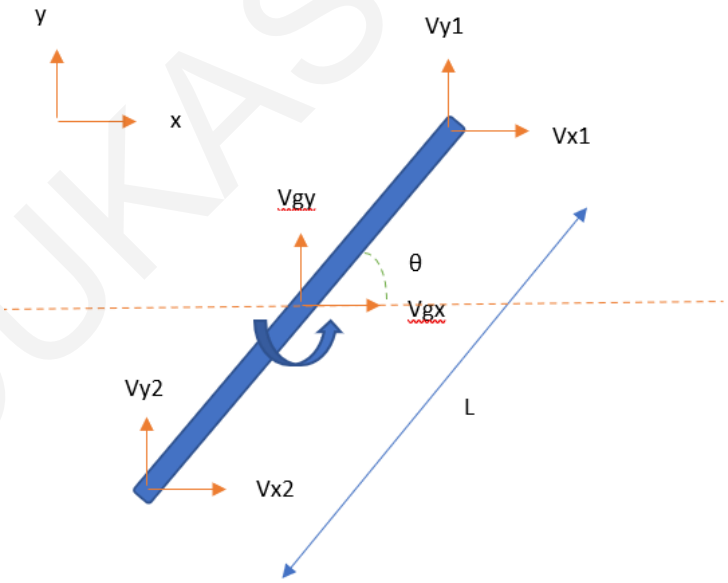

$$V_{x1} = V_{gx} - \omega \frac{L}{2} sin\theta$$

$$V_{y1} = V_{gy} + \omega \frac{L}{2} cos\theta$$

$$V_{x2} = V_{gx} + \omega \frac{L}{2} sin\theta$$

$$V_{y2} = V_{gy} - \omega \frac{L}{2} cos\theta$$

Figure 45: Free body diagram of the link.

Figure 47 shows the results of a simulation for a 2.97s long pulse voltage input activated at 0.5s, as well as the temporal response for the two joint angles and slider position. The simulation represents the first step of the sequence one on horizontal motion. The motor is turned on and the links begin to move to their final configuration in about 2.47s. Figure 46 represent a sketch of the initial and the final stage of the mechanism during the configuration and the Table 7 shows the parameters used for the simulation. By locking the join three the two links 2a and 2b which presented with orange color form an effective link (2).

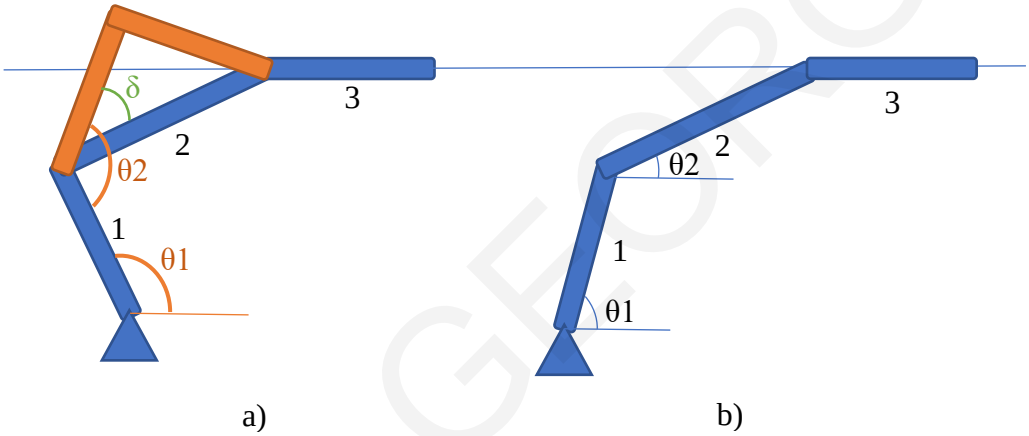

a) b)

Figure 46: Sketch of the: a) initial form of the mechanism, b) final form of the mechanism.

In 20sim the angle was given us the absolute angle of the link from the horizontal surface. In order to compere the 20sim results with the experimental results am equation was developed to convert the angles.

$$\theta_2 = \theta_2 - \delta - (180 - \theta_1)$$

Table 7: Simulation parameters.

Name	Value	Quantity	Unit	Description	Arithmeti...
B_sl\r	0.2				Real
B\r	3.0e-4				Real
C\c	1.0e-10				Real
Jsh\j	4.9e-5				Real
k_m\r	0.5				Real
La\j	0.033				Real
Link1\J\j	7.27e-4				Real
Link1\L_2c\K	0.1			gain	Real
Link1\L_2s\K	0.1			gain	Real
Link1\m_break_1x\j	0.361				Real
Link1\m_break_1y_g\effort	-3.54				Real
Link1\m_break_1y\j	0.361				Real
Link1\m_break_2x\j	0.361				Real
Link1\m_break_2y_g\effort	-3.54				Real
Link1\m_break_2y\j	0.361				Real
Link1\m_g\effort	-2.139				Real
Link1\m_x\j	0.218				Real
Link1\m_y\j	0.218				Real
Link2\J\j	0.00393				Real
Link2\L_2\C	0.329			output value	Real
Link2\m_break_1x\j	0.361				Real
Link2\m_break_1y_g\effort	-3.54				Real
Link2\m_break_1y\j	0.361				Real
Link2\m_break_2x\j	0.361				Real
Link2\m_break_2y_g\effort	-3.54				Real
Link2\m_break_2y\j	0.361				Real
Link2\m_g\effort	-4.28				Real
Link2\m_x\j	0.436				Real
Link2\m_y\j	0.436				Real
m_sl\j	0.218				Real
n_screw\r	3.98e-4				Real
Pulse\amplitude	51.5	Magnitude	none		Real
Pulse\start_time	500.0 {ms}	Time	second		Real
Pulse\stop_time	2.97 {s}	Time	second		Real
R1\r	0.1				Real
R2\r	0.1				Real
R3\r	0.1				Real
Ra\r	0.75				Real
S_Vx2\flow	0.0				Real
S_Vy1\flow	0.0				Real
S_Vy2\flow	0.0				Real

The time response for the two absolute angles and the slider position are shown in the Figure 47. The two angles are the same as the angles calculated in the experimental studies. The initial angles θ_i and the final angles θ_f of step 1, sequence 1 in horizontal motion are:

$\boldsymbol{\theta_i}$ = [103.01, 134.18] degrees
$\boldsymbol{\theta_f}$= [73, 25] degrees

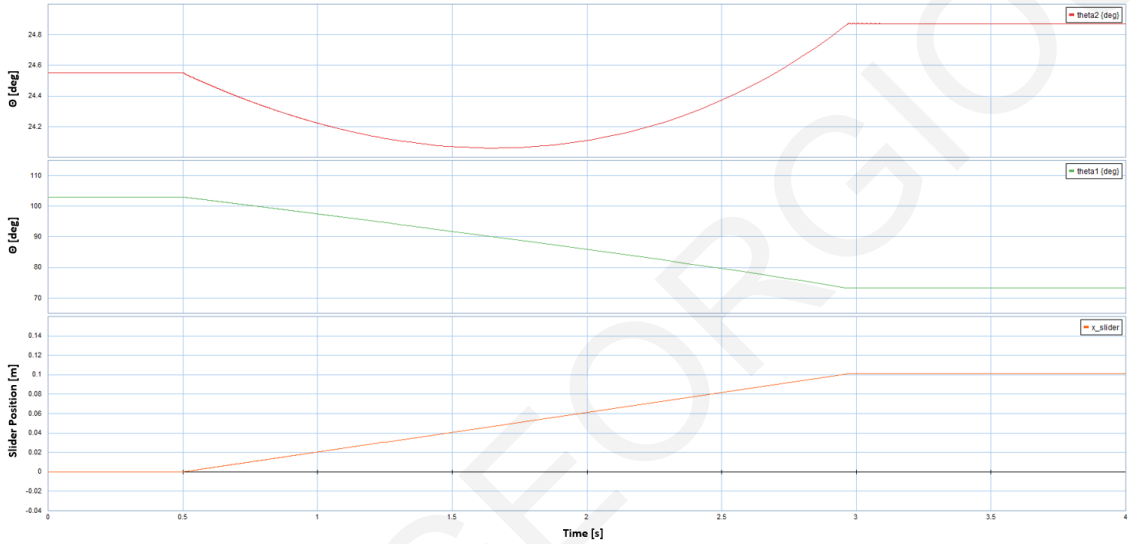

Figure 47: Time response for a pulse voltage input to the motor. Green line represents the angle 1, red line the angle 2 and orange line the slider position.

The objective of this study was to reduce the model complexity of the system as the accuracy stays the same. Element power was used to calculate a metric to reduce the model complexity. For a system with a total of N_e ideal energy elements, for n^{th} element, element activity and the non-dimensional element activity index are defined as:

Element activity $$A_n = \int_0^T |P_n(t)|\, d_t$$

Non-dimensional element activity index $$EAI_n = \frac{Activity_n}{\sum_{j=1}^{N_e} Activity_j}$$

Table 8 shows the element activities of the system. The activity of each item is a measure of the importance between of each item. The activities of the elements were entered in a significant order according to their importance, as shown in Table 8. Listed first is the element with the greatest energy and listed last the most insignificant element with the least energy. To simplify the model, the elements that are not so important can

be eliminated and only those whose energy coincides up to 99% remain. The four first elements can change the behavior of the system as there are critical elements depends on there activity. The elements that are shaded with gray color are the elements that were judged the least important in the system. The most important element is the inertia (Jsh) of the screw slider and the less important element is the masses (Link1_m_break_2x) and (Link2_m_break_1y) with zero activity because there was no movement in those points.

Table 8: System elements activity and activity index.

Element	Acticity	Activity index
Jsh	11.23524071	46.3640999
B	7.95678216	32.8349924
La	4.53136272	18.6994261
Ra	0.41928480	1.7302489
Link2_m_x	0.01533763	0.0632933
Link2_m_break_1x	0.01311172	0.0541077
Link1_m_break_1x	0.01269120	0.0523724
Link2_m_break_2x	0.01269120	0.0523724
R2	0.01153219	0.0475895
R1	0.01116748	0.0460845
m_sl	0.00791788	0.0326745
Link1_m_x	0.00186755	0.0077067
B_sl	0.00084026	0.0034675
Link2_m_break_2y	0.00079141	0.0032659
Link1_m_break_1y	0.00079141	0.0032659
Link1_J	0.00066138	0.0027293
Link2_m_y	0.00023896	0.0009861
Link2_J	0.00014130	0.0005831
Link1_m_y	0.00012761	0.0005266
R3	0.00003112	0.0001284
Link1_m_break_2y	0.00001914	0.0000790
Link1_m_break_2x	0.00000000	0.0000000
Link2_m_break_1y	0.00000000	0.0000000

In this chapter, a simpler system of the mechanism has been proposed which illustrates a crank slider mechanism. The system was modeled and a bond graph was great. From the analysis the time response for a pulse voltage input to the motor was calculated and the activities of the elements consisting the system was calculated.

Chapter 5

5 CONCLUSIONS

Adaptive Architecture is of great importance because of its various benefits to the functionality of buildings. In general, although this innovation is in its early stages it can aid the development of technologies for the control of systems as well as for the way they are manufactured.

Before we go into implementation on a scale of 1 to 1 it is important to have experimental tests on a small scale. As part of this need, an experimental device has been created with which preliminary tests have been carried out. Through this Master's thesis, the experimental arrangement has been implemented and optimized to make more extensive and analytical studies. Compared to previous versions, the structure of the mechanism has been upgraded with the integration of optical encoders. Also, the whole system has been redesigned and implemented, with a new program that has been deemed suitable for research purposes, as well as more accurate measurements provided by the position sensors, allowing for more in-depth studies before the model is made on a scale of 1 to 1. Upgrade on the wiring, the power system, the control program were implemented. The graphic user interface is friendlier and a new card is controlling the robotic mechanism and giving it access to a wider range of actions and features.

Based on the coupled 1-DOF mechanisms, a proposal has been made for the remodeling of architecture buildings. The applicability and potential of the methods has been confirmed by simulations and experimental studies. The established structure is appropriate for the execution of adaptive architecture since it allows for that the shape of buildings to be altered automatically by external input. In this manner, is considered a great contribution to the field of Adaptive Architecture which has great prospects.

Besides reconfigurability, further design features exist and are to be considered among with erectability, foldability, expandability, transportability, and modularity. It is noted that these issues are significant and will be further investigated. In regards of the architectural design, adaptability and creativity is the proposed approach and the variety of unique design parameters can be adjusted in regard to the length, shape, and number of the separate members of the structural mechanism. It is worth mentioning that designs such as uneven installation of levels as well as a span alteration of the building (specific distance in between the ground supports) can easily be adapted to the installation's site requirements.

The single motion actuator is among the main advantages of the suggested method although, a requirement for the proposed method is the efficient brakes system. For this purpose, new breaking methods may be developed such as customized discrete-position, pinned-brake systems.

Adaptive architecture and reconfigurability, are a multidisciplinary field that got their knowledge from structural engineering, control, robotics and architecture. It is a new scientific field filled with unlimited possibilities!

Bibliography

[1] Christoforou, E., Müller, A., and Phocas, M., 2012, "Motion Planning for Shape-Controlled Adaptable Buildings Resembling Topologically Closed-Loop Robotic Systems," ASME Paper No. DETC2012-70177.

[2] Christoforou EG, Müller A, Phocas MC, Matheou M, Arnos S. Design and control concept for reconfigurable architecture. Mechanical Design 2015; 137: 042302-1 – 042302-8.

[3] d'Estee Sterk, T., 2006, "Shape Control in Responsive Architectural StructuresCurrent Reasons and Challenges," Fourth World Conference on Structural Control and Monitoring, pp. 1–8.

[4] Kirkegaard, P., and Foged, I. W., 2010, "Development and Evaluation of a Responsive Building Envelope," International Adaptive Architecture Conference, pp. 1–9.

[5] Christoforou, Eftychios G.; Müller, Andreas; Phocas, Marios C.; Matheou, Maria; Arnos, Socrates (2015). Design and Control Concept for Reconfigurable Architecture. Journal of Mechanical Design, 137(4), 042302–. doi:10.1115/1.4029617 .

[6] Christoforou, E., Müller, A., Phocas, M., Matheou, M., and Arnos, S., 2013, "Towards Realization of Shape-Controlled Adaptable Buildings Following a Robotics Approach," ASME Paper No. DETC2013-12885.

[7] M.C. Phocas, E.G. Christoforou, C, Theokli, K. Petrou. Reconfigurable linkage structures and photovoltaics integration. Journal of Building Engineering (Elsevier), 43, 2021.

[8] Christoforou, E.G., Georgiou, L., Phocas, M.C., Louca, L.S., Müller, A. (2022). A Robotics Perspective on Architecture: Modelling and Control of Reconfigurable Buildings. In: Müller, A., Brandstötter, M. (eds) Advances in Service and Industrial Robotics. RAAD 2022. Mechanisms and Machine Science, vol 120. Springer, Cham. https://doi.org/10.1007/978-3-031-04870-8_34.

[9] Karnopp, D.C., Margolis, D.L., D., Rosenberg, R.C.: System Dynamics: Modeling and Simulation of Mechatronic Systems. John Wiley and Sons, Inc., New York (2012).

[10] Louca, L.S., Stein, J.L., Hulbert, G.M.: Energy-Based Model Reduction Methodology for Automated Modeling. Journal of Dynamic Systems Measurement and Control, 132(6), 061202 (2010).

[11] Controllab Products BV, 20-sim Pro Users' Manual, Version 3.6. The University of Twente - Controllab Products BV. Enschede, The Netherlands (2005).

Appendices

Appendix I – Drawings for building the parts of the robotic mechanism

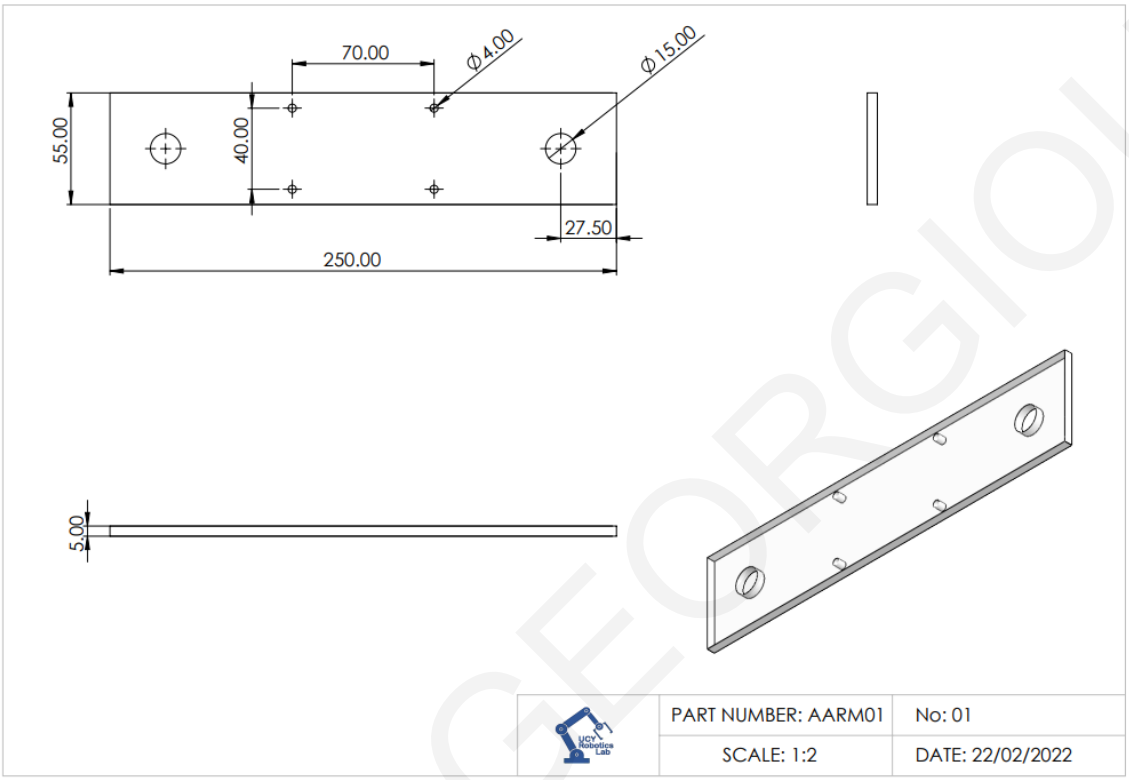

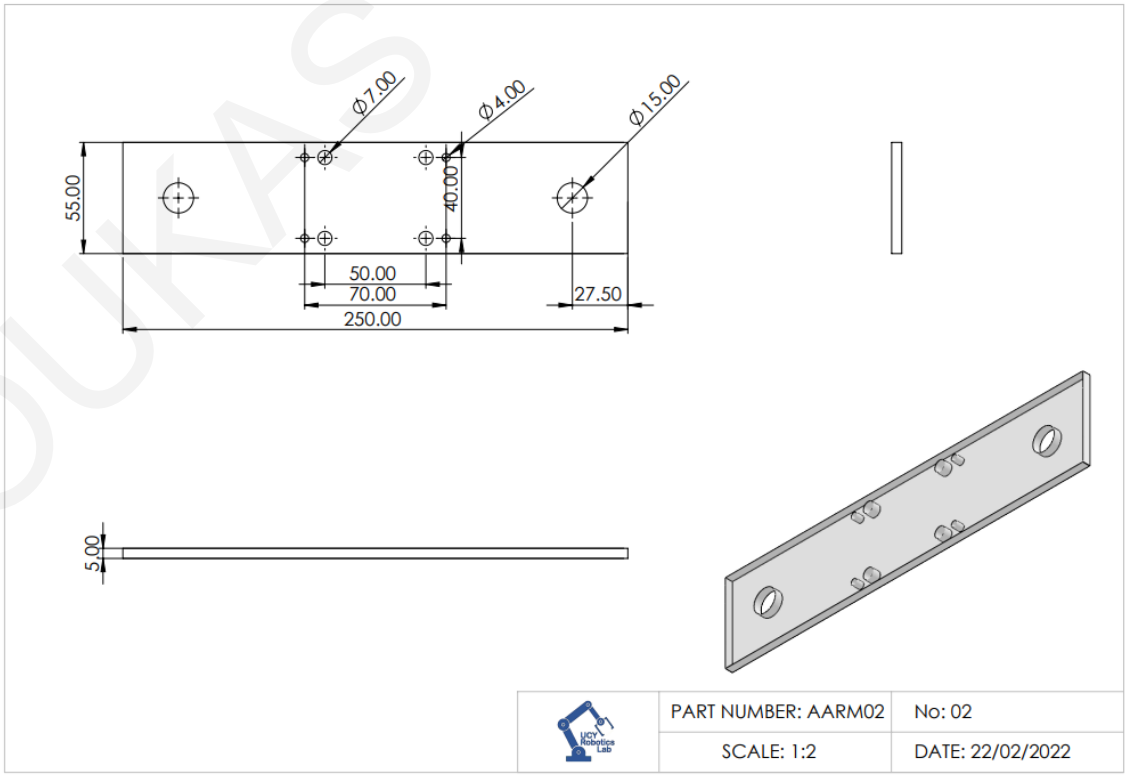

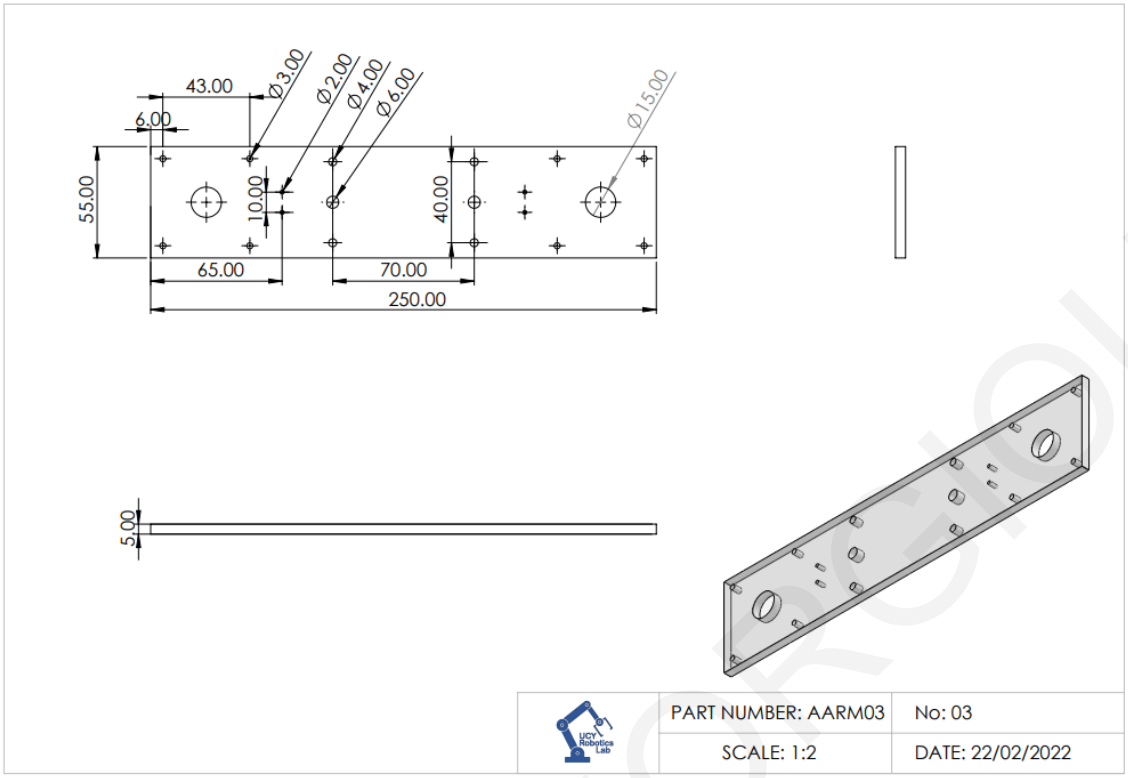

UCY Robotics Lab	PART NUMBER: AARM03	No: 03
	SCALE: 1:2	DATE: 22/02/2022

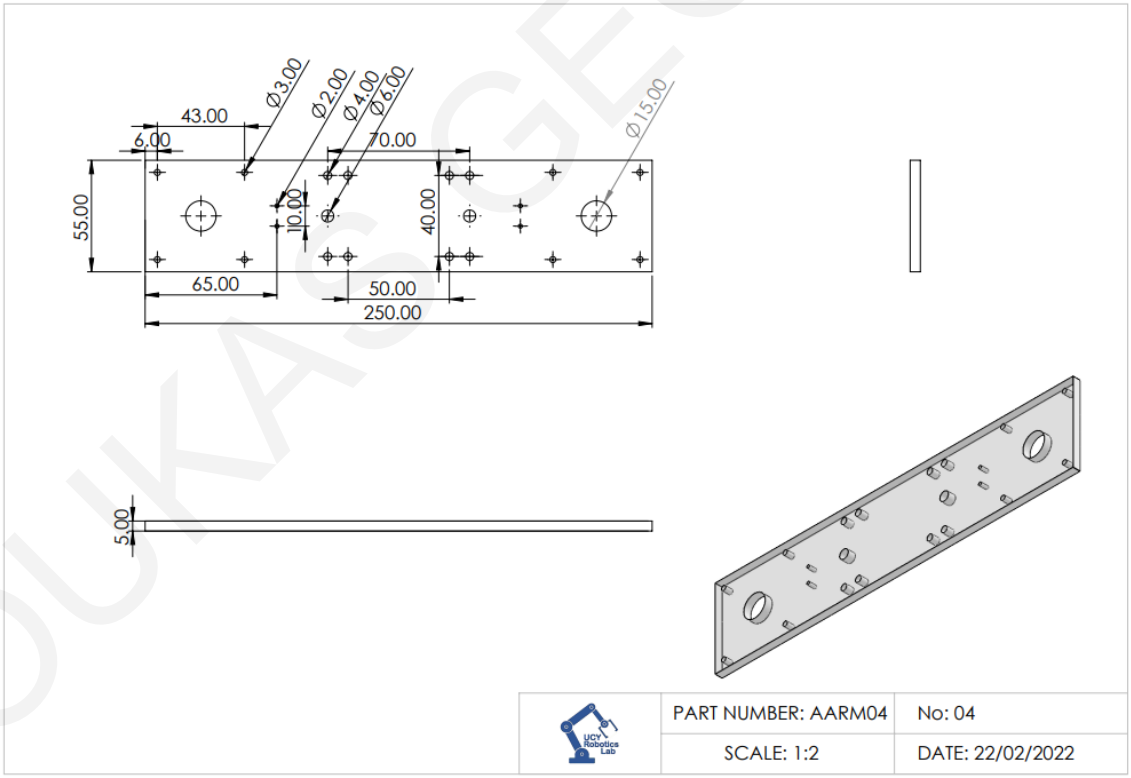

UCY Robotics Lab	PART NUMBER: AARM04	No: 04
	SCALE: 1:2	DATE: 22/02/2022

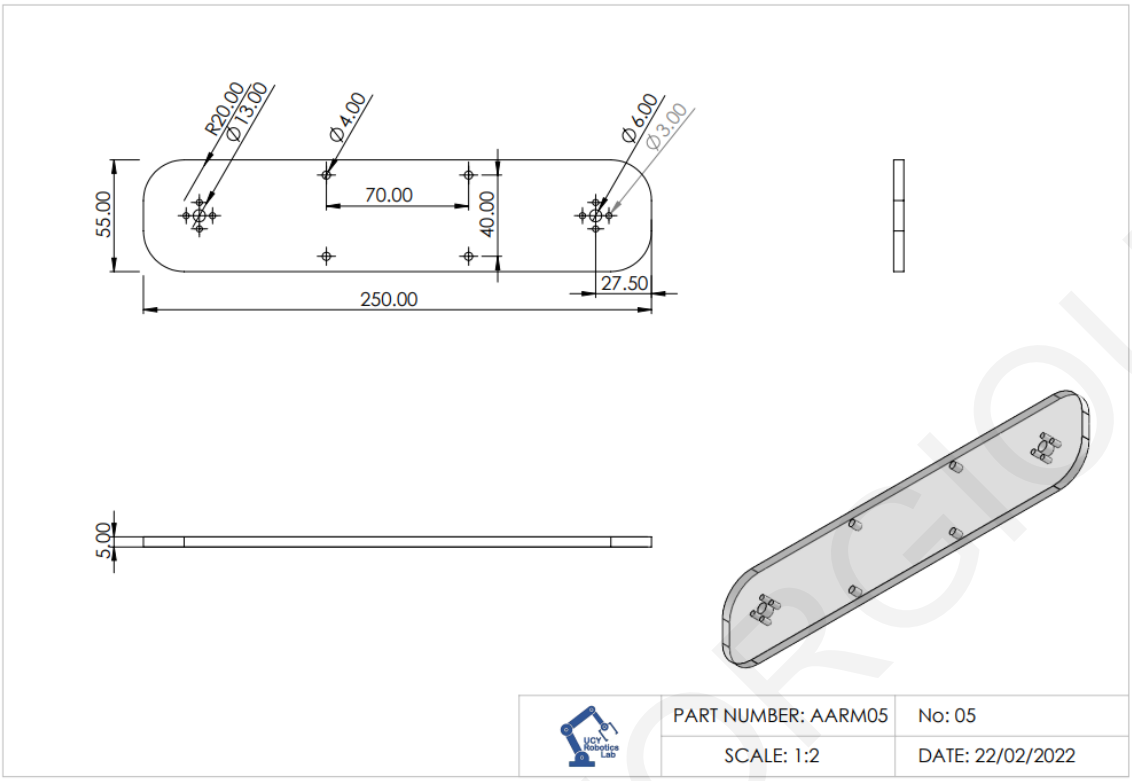

	PART NUMBER: AARM05	No: 05
	SCALE: 1:2	DATE: 22/02/2022

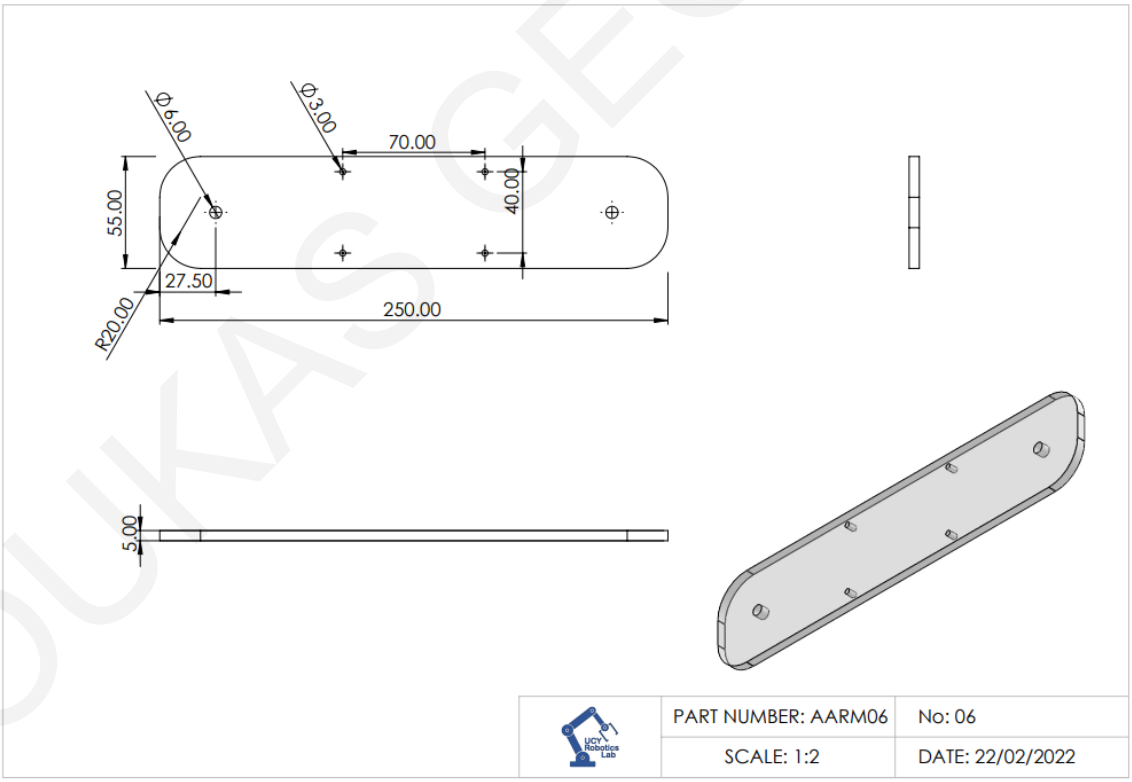

	PART NUMBER: AARM06	No: 06
	SCALE: 1:2	DATE: 22/02/2022

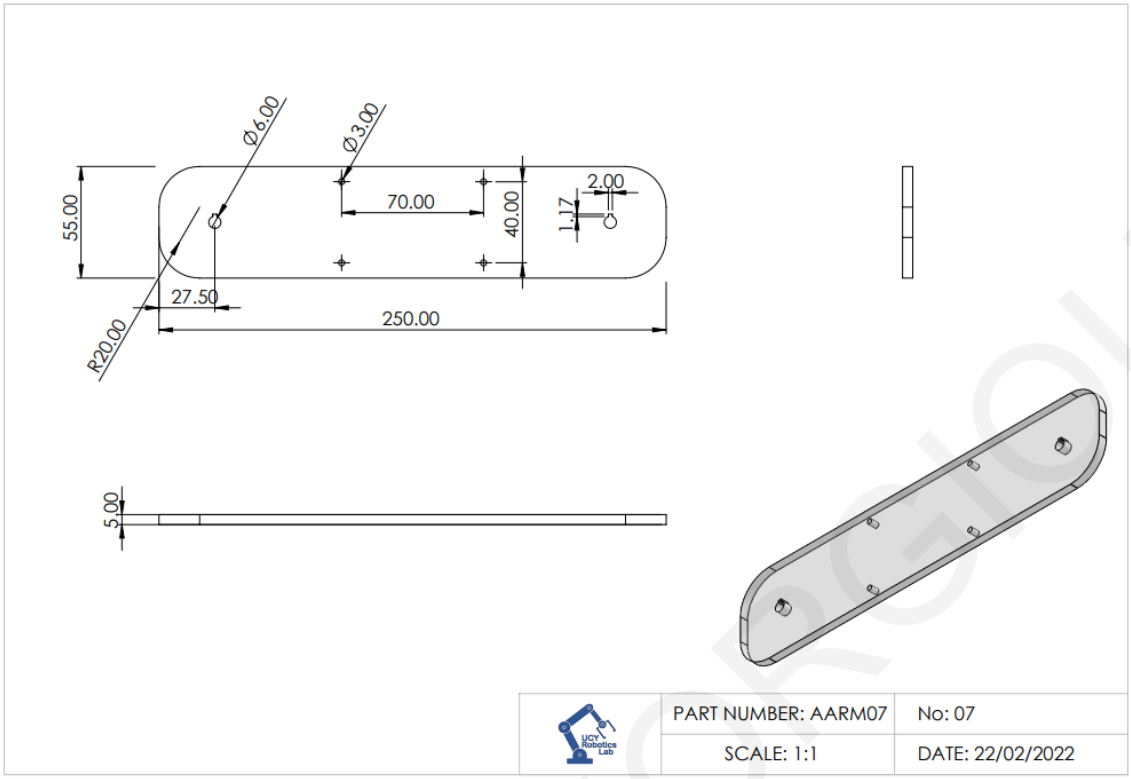

	PART NUMBER: AARM07	No: 07
	SCALE: 1:1	DATE: 22/02/2022

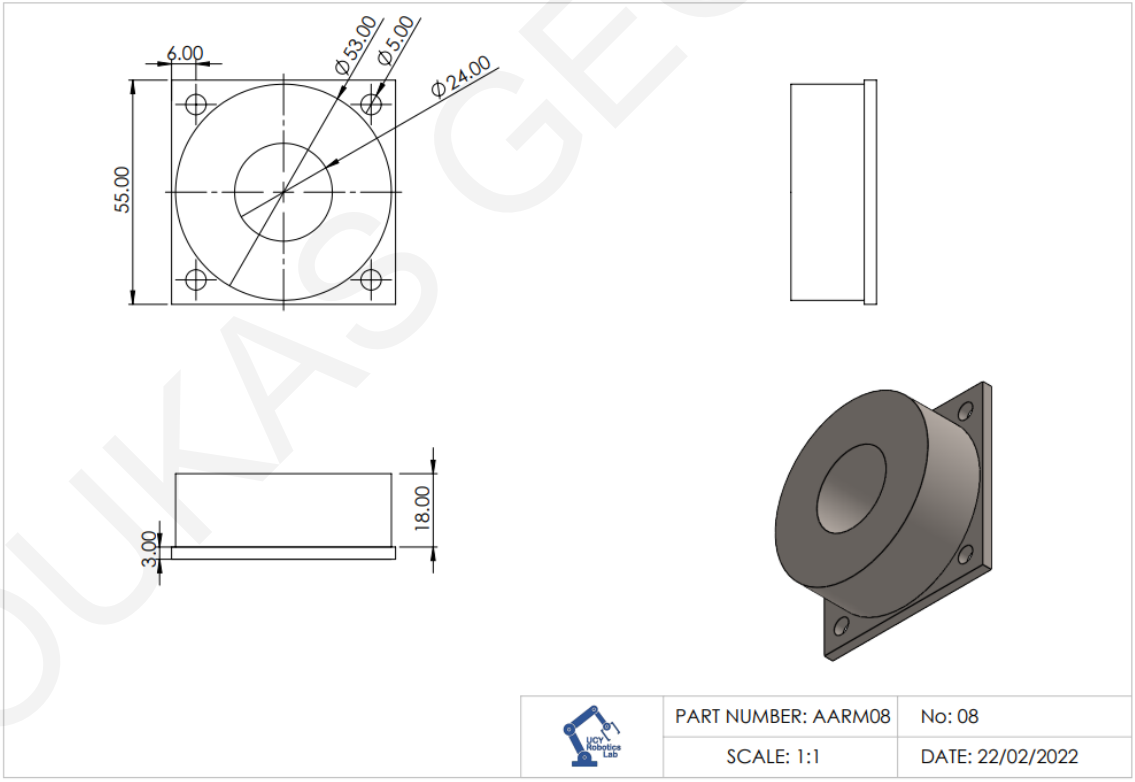

	PART NUMBER: AARM08	No: 08
	SCALE: 1:1	DATE: 22/02/2022

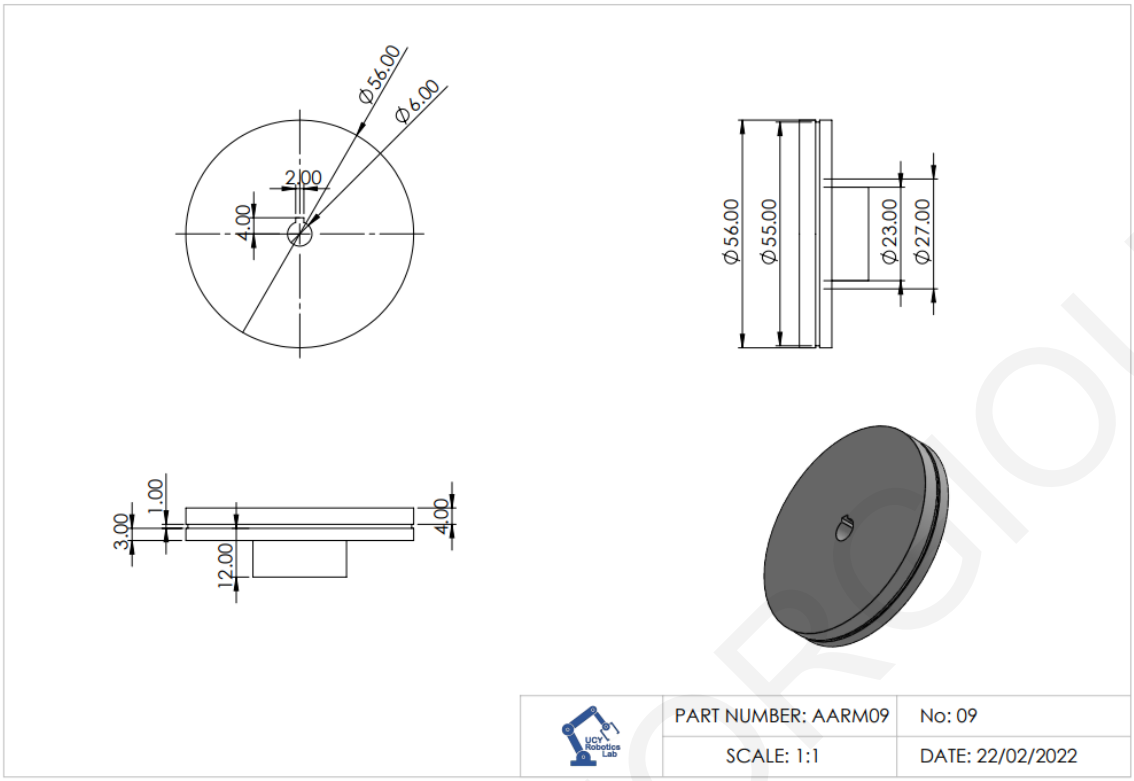

	PART NUMBER: AARM09	No: 09
	SCALE: 1:1	DATE: 22/02/2022

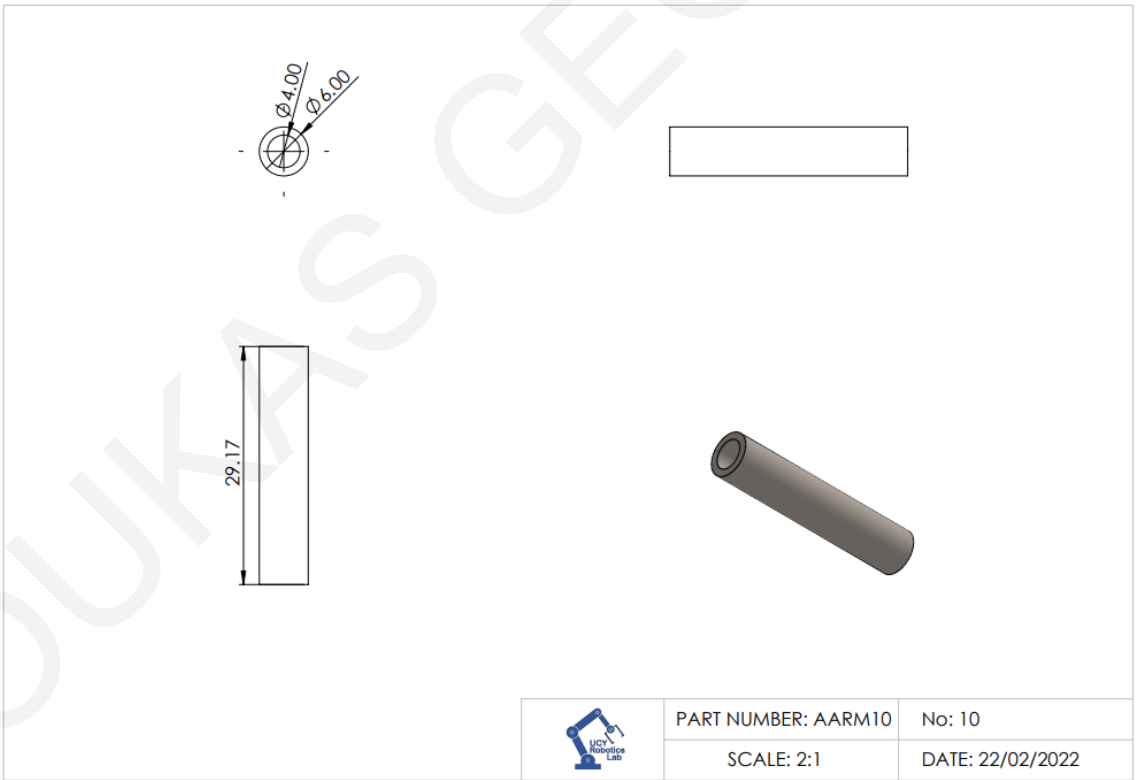

	PART NUMBER: AARM10	No: 10
	SCALE: 2:1	DATE: 22/02/2022

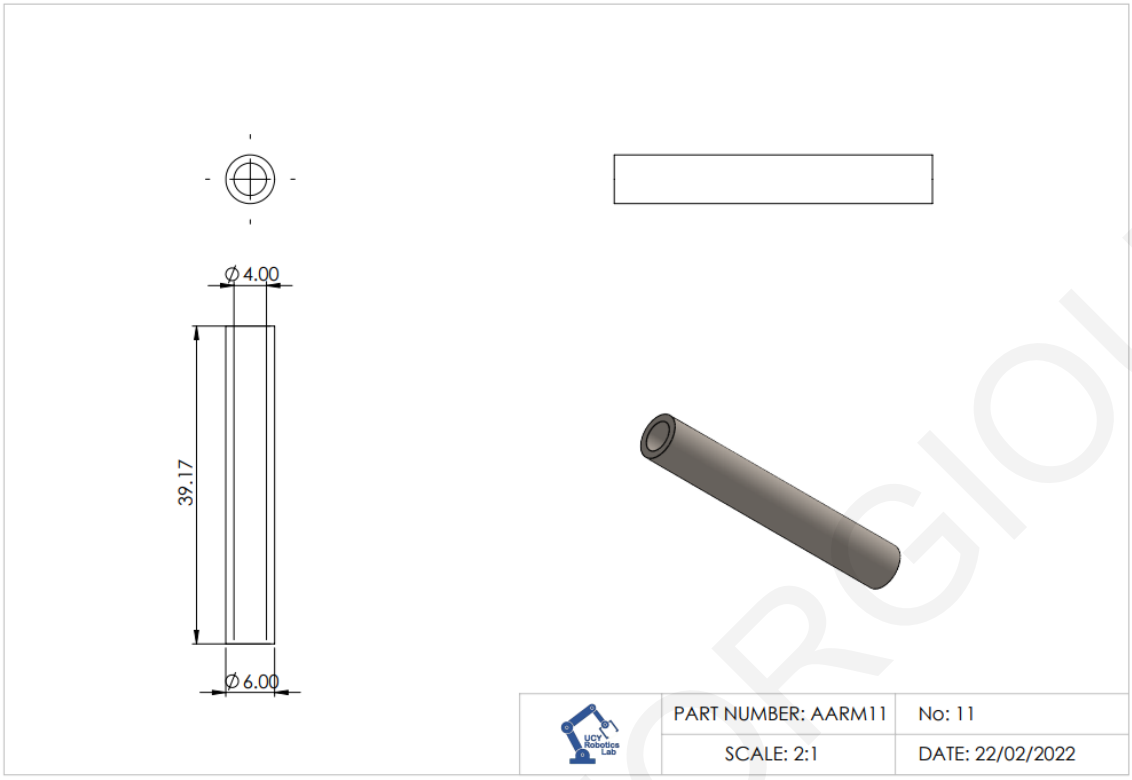

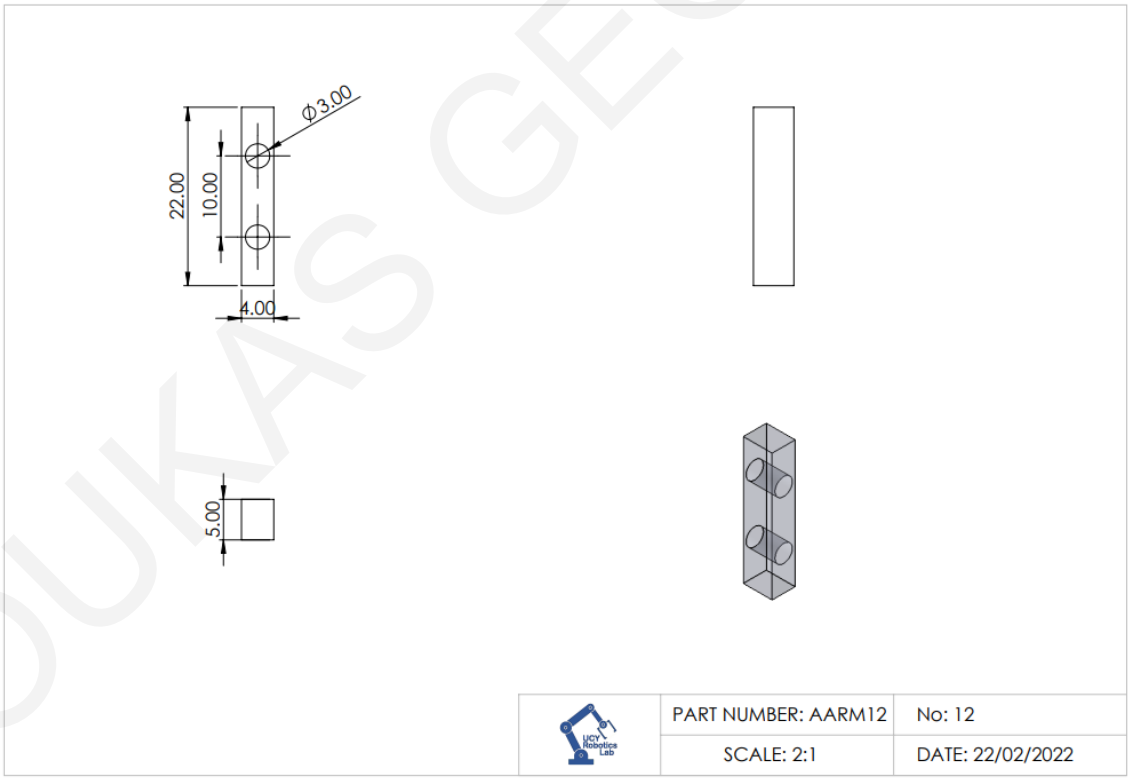

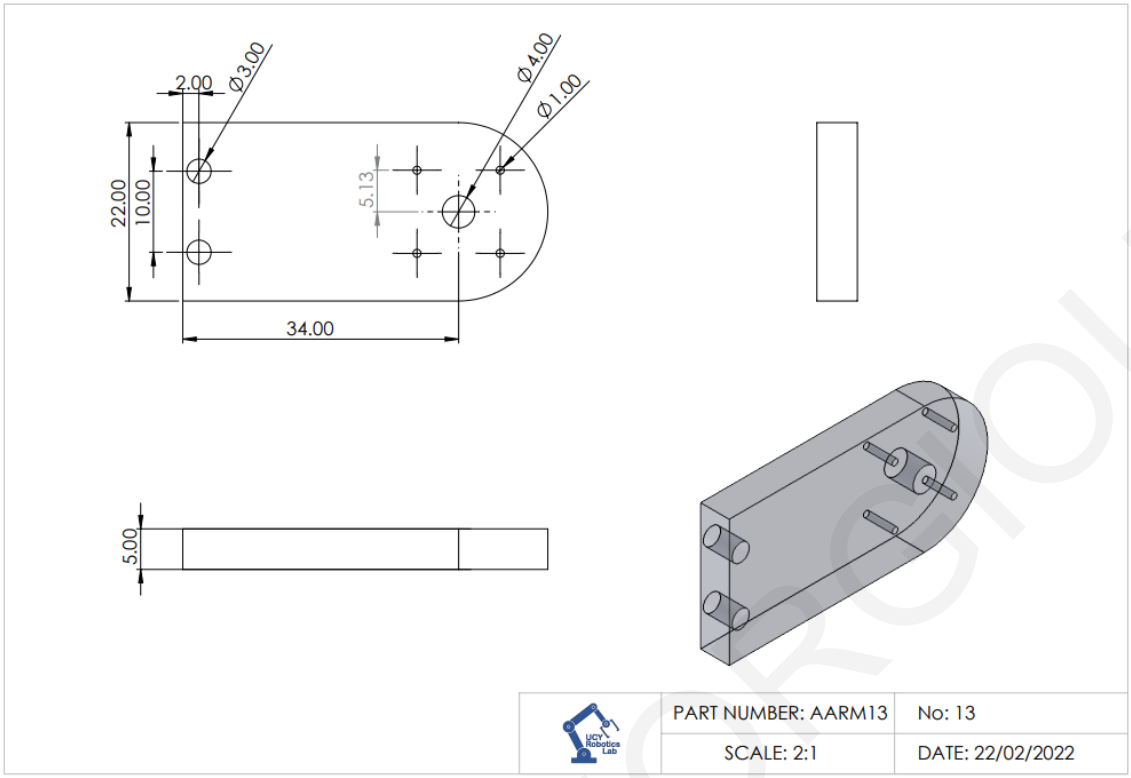

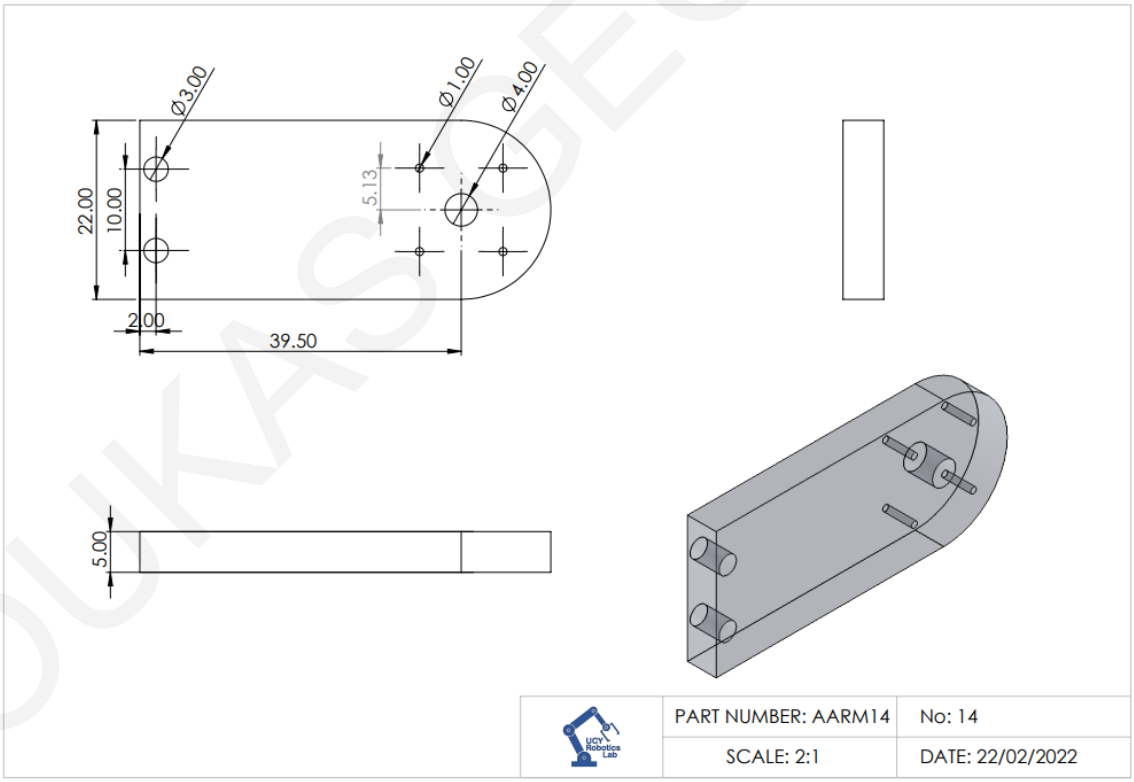

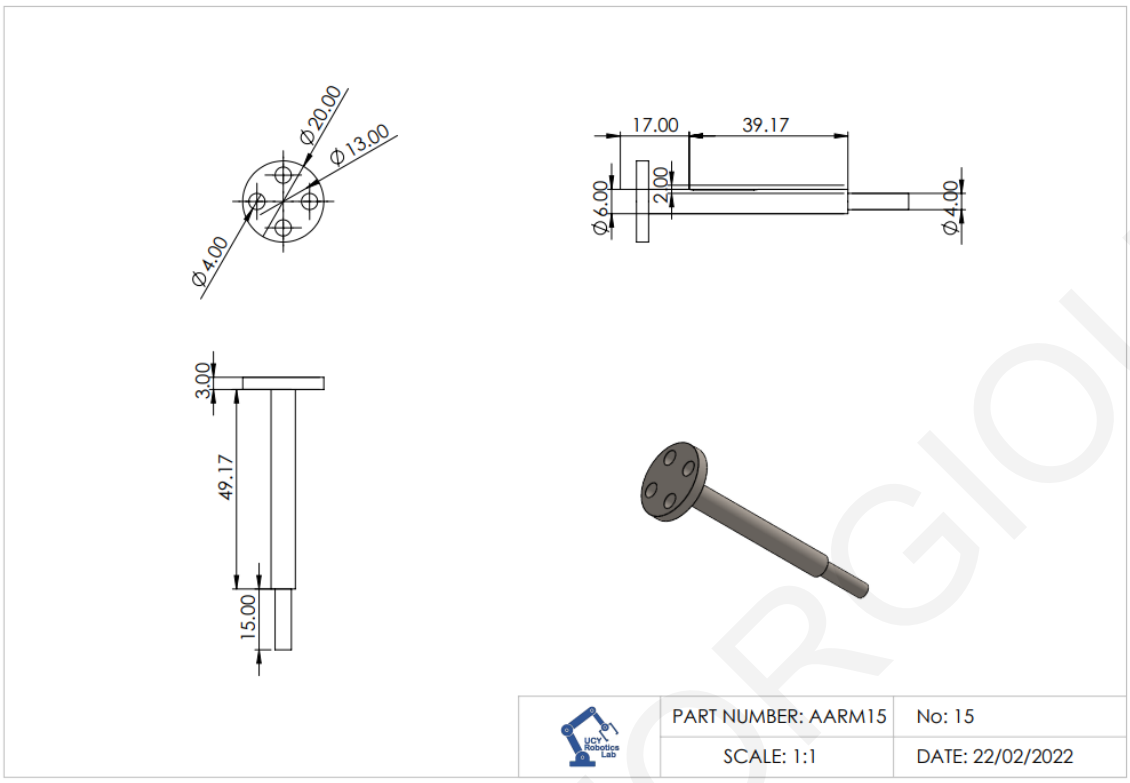

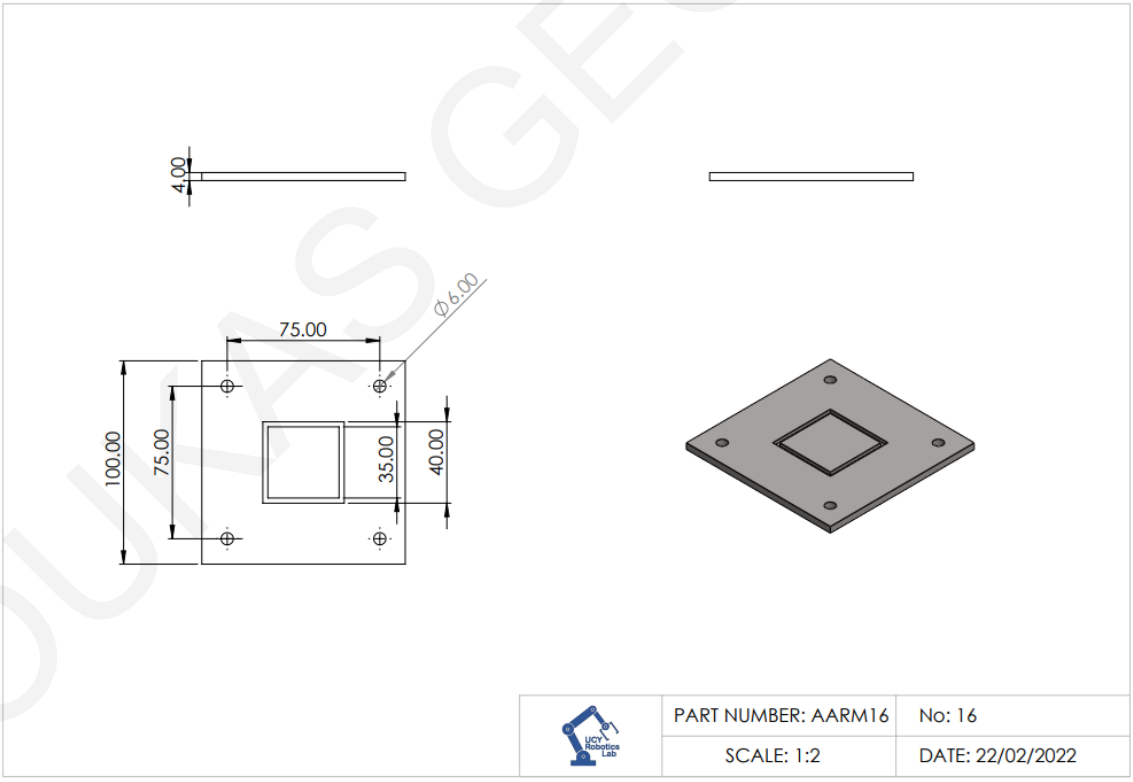

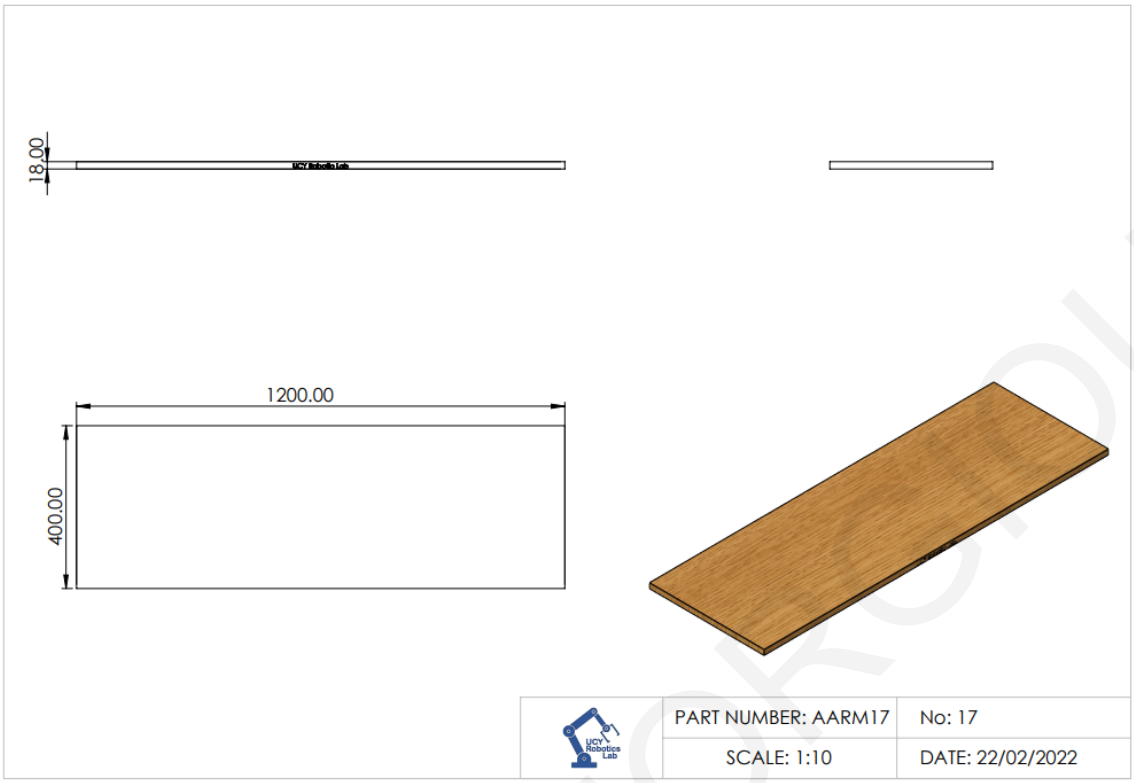

Appendix III – Data Sheets

[1]

1.8° 42MM High Torque Hybrid Stepping Motor

Item	Specifications
Step Angle	1.8°
Step Angle Accuracy	±5% (full step, no load)
Resistance Accuracy	±10%
Inductance Accuracy	±20%
Temperatru Rise	80°CMax. (rated current,2 phase on)
Ambient Temperatuar	–20°C~+50°C
Insulation Resistance	100M?Min.,500VDC
Dielectric Strength	500VAC/ for one minute
Shaft Radial Play	0.02Max. (450 g–load)
Shaft Axial Play	0.08Max. (450 g–load)
Max. radial force	28N (20mm foom the flange)
Max.axial force	10N

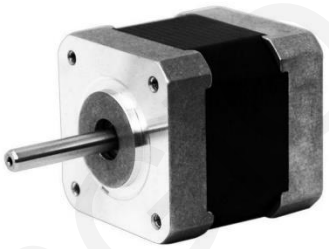

● 42MM Hybrid Stepping Motor Specificatiors

Model No	Rated Voltage	Current /Phase	Resistance /Phase	Inductance /Phase	Holding Torque	# of Leads	Rotor Inertia	Weinght	Detent Torque	Length
XY42STH34-0354A	V	A	Ω	mH	Kg–cm		g–cm²	kg	g–cm	mm
	12	0.35	34	33	1.6	4	35	0.22	120	34

● Dimension

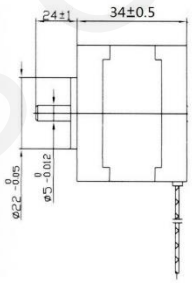

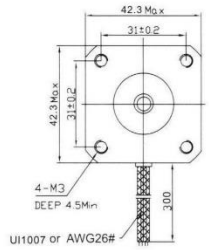

● Wiring Diagram

4 LEADS

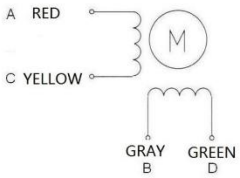

● Pull out Torque Curve

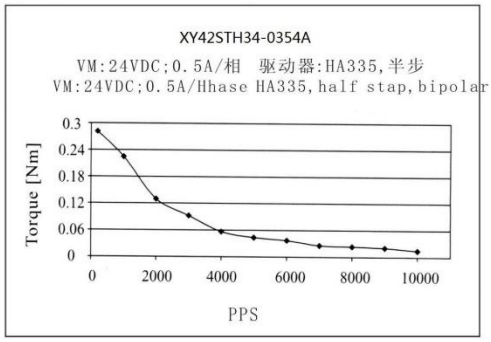

TB6600 Stepper Motor Driver

Analog Driver
Model TB6600

Analog Technology, max. 40 VDC / 4.0 A (PEAK)

Product Description:
The TB6600 single axis drive is a low cost microstepping drive. It is suitable for driving 2-phase and 4-phase hybrid stepper motors. Not for professional applications.

Features:

- Cost-effective
- Supply voltage up to +40 VDC, Output current up to 4.0 A (PEAK)
- Output current selectable in 8 steps via DIP-switch
- Automatic idle-current reduction (in standstill mode) to reduce motor heating
- Pulse input frequency up to 20 kHz
- Input suitable for 5 V signals
- Inputs are optically isolated
- 6 selectable microstep resolutions, up to 6400 steps/rev with standard 1.8° motors
- Suitable for 2-phase and 4-phase motors
- Supports PUL/DIR mode
- Over current and overheat protection

Electrical Specifications:

Parameters	Min	Typ.	Max	Unit
Output current	0.7	-	4.0 (3.5 RMS)	A
Supply voltage	+9	+36	+40	VDC
Logic signal current	8	10	15	mA
Puls input frequency	0	-	20 when duty cyle is 25 high / 75 low 13 when duty cycle is 50 / 50	kHz
Insulation resistance	500			MΩ

Further Specifications:

Microsteps / 1,8 °	200		6400
PUL / DIR		yes	
NEMA sizes	17		24
Motor type Mecheltron	42BYGH-XXXX		60BYGH-XXX

22.01.18

Right of techn. modifications is reserved www.sorotec.de Technische Änderungen vorbehalten

TB6600 Stepper motor driver

Analog Driver

Model TB6600

Mechanical Specifications: (Unit: mm)

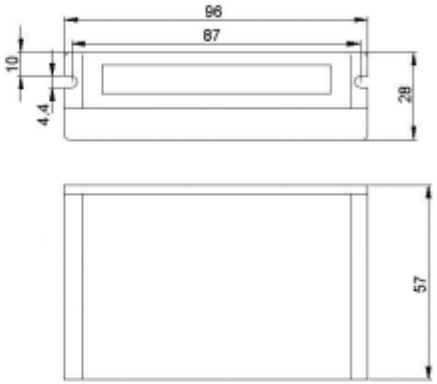

Applications:

Suitable for a wide range of stepping motors of NEMA sizes 17, 23 and 24 (42x42 mm to 60x60 mm). It can be used in various kinds of machines, such as X-Y tables, engraving machines, labeling machines, laser cutters, pick-place devices, and so on. Particularly well suited for applications where low noise levels, less heat development, high speed and high precision are desired.

Typical Connection Schematic:

A typical system consists of stepper motor, stepper motor driver, power supply and controller. The following image shows a typical connection schematic:

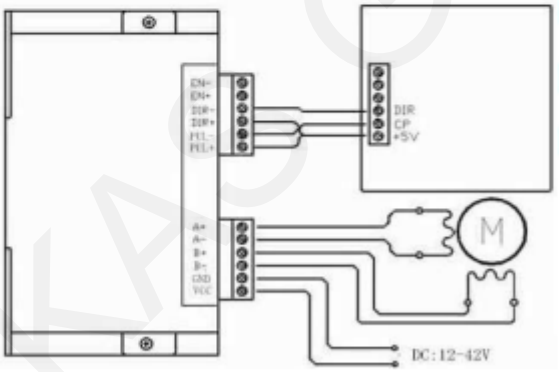

Logic control signals which have 5 V can be connected directly;
R 1kΩ must be connected in line when control signal is 12V;
R 2kΩ must be connected in line when control signal is 24V to ensure control signal current is 8mA to 15mA. 22.01.18

Professional Encoder Manufacturer

HKT22 SERIES

Wuxi REP Technology co., Ltd.
Add.: #6 Gaikai Rd., 214124 Wuxi, China
Tel: +86-510-8562-5086
Fax: +86-510-8224-4577
Email: info@hedss.com.cn

◆ Feature

HKT22 is a 2-channel low cost optical hollow shaft encoder which can be fixed easily on shafts of motors. HKT22 has 2 square-wave outputs which are 90-degree phase shifted for counting and direction information.

◆ Specifications

Electrical Specifications	
Output Wave	Square Wave
Current Consumption	≤50mA
Output Current	2~12mA
Response Frequency	0~30KHz
Output Phase Difference	90° ± 45°
Output Voltage	-0.5V~Vcc
Signal Level	$V_H \geq 85\% Vcc, V_L \leq 0.3V$
Mechanical Specifications	
Rotor Inertia Of Code-wheel	$4.0 \times 10^{-6} Kgm^2$
Shock Resistance	$980 m/s^2$, 6ms, 2 times each on XYZ
Vibration Proof	$50 m/s^2$, 10~200Hz, 2 hours each on XYZ
Working Life	MTBF≥50000h (+25℃, 2000rpm)
Weight	10g (with 0.5m cable)
Environmental Specifications	
Working Humidity	30~85% (no condensation)
Storage Temperature	-40℃~85℃
Working Temperature	-10℃~85℃

◆ Terminal Assignment

Flat Cable (from the colored end)	1	2	3	4	5
Voltage Output	0V	N.C	Ch.B	+5V	Ch.A

Professional Encoder Manufacturer

HKT22 SERIES

◆ Ordering Information

HKT22 XX – 702 C1 – XXX B – 5 E

Series
HKT22 Series

Bore Size
φ2mm 02
φ3mm 03
φ4mm 04

Glass code-wheel 702

Connector
C1-Flat Cable Connector

Resolution Number
100, 120, 200, 256, 300, 360, 400, 500

Outputs
B 2-Channel outputs

Supply Voltage
5 5V DC

Output Circuit
E Voltage output

◆ Dimension Diagram

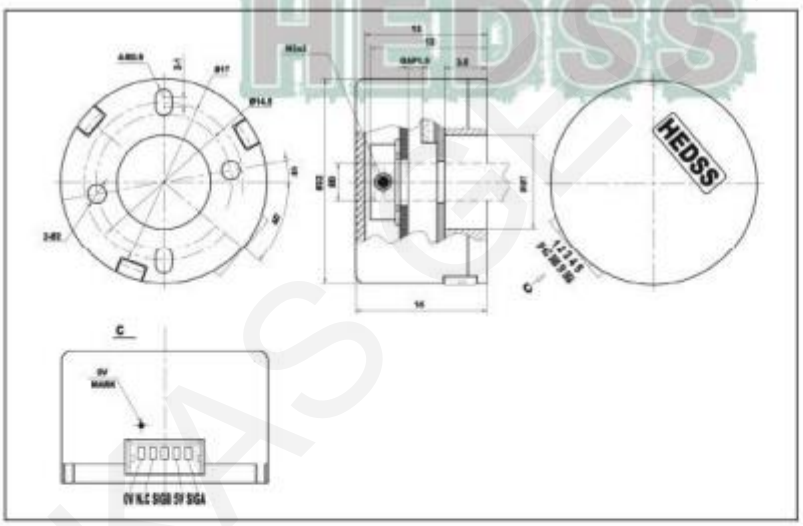

Flange Mounted Power On Brake

TYPE 52

Tel: +44 (0)1388 770 360 | sales@sgtransmission.com
www.sgtransmission.com

SG Transmission

The flange mounted power on brake, also known as a single-surface or single-disc brake, generates a braking effect when the coil is energised. The brake body is mounted on the drive and when energised (working current) with nominal voltage, the armature disc is attracted through the minimal air gap to generate a static braking effect.

This power on brake is typically used to safely stop and hold a rotating force in position. Due to the integrated, abrasion-resistant and asbestos-free brake lining, it can also be used for dynamic braking applications. The force can be regulated up to the nominal voltage by an external voltage regulator.

The durable construction of this brake means that it is essentially zero backlash (torsionally rigid) creating an increased level of safety and accuracy.

Benefits

- Backlash free
- Long life expectancy
- Durable construction
- Low maintenance

Features

- Customisable
- High toque (multi pole) versions available
- Special voltages/forces/mountings available on request
- Insulation class F/H (155°c) as standard or higher on request
- Manufactured and tested to DIN VDE 0580
- Made in the UK

Key applications

- Machinery
- Material handling
- Warehouse logistics
- Military
- Security
- Medical

SIZE	FIELD MOUNTING	ARMATURE TYPE	BORE	D.C. VOLTAGE
12	BRAKE	F.M	C.R	25	24

SG Transmission, 20 Longfield Road, South Church Enterprise Park, Bishop Auckland, County Durham, UK, DL14 6XB ISSUE 003

Technical data

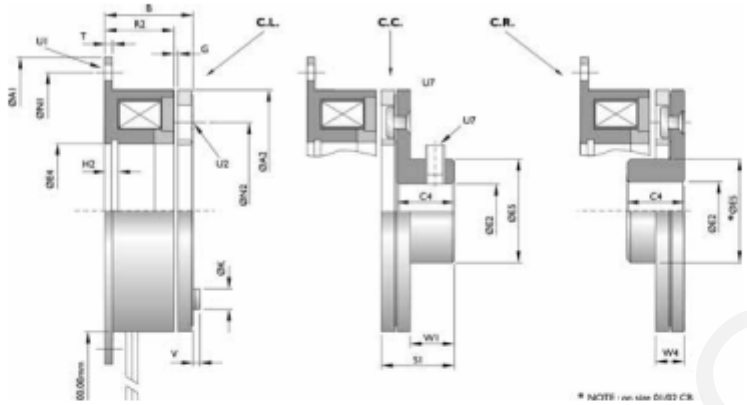

Size	Torque TS (Nm)	Max P20 (w)	A1 H9	A2	B	C4	Max E2 H7	E4 H8	E5	G	H2	K	N1	N2	R2	S1	T	U1 x4	U2	U7	V	W1	W4
00	0.30	5	38	28.6	17	7	6.5	11	10	0.1	-	5	33.3	19.5	14	9.7	1.5	3.2	2x2.6	M3	1	4.5	4.7
01	0.60	6	38	30	18.5	10	6.5	11.5	12	0.1	-	5	33.3	19.5	16	12.8	1.5	2.6	2x2.6	M3	1	8	-
02	0.75	6	45	32	19.5	10	6.5	13	12	0.1	3	5	38	23	17	12.8	2	3.5	3x2.6	M3	1.5	8	4.8
03	1.20	8	54	40	23.2	12	10	19	17	0.15	3.2	6.1	47	30	20	15.3	2	3.5	3x3.1	M3	1.5	9.5	5.8
04	1.60	8	62	42	23.2	12	10	16	17	0.15	-	6.1	54	29	20	15.3	2	5	2x3.1	M3	1.5	9.5	5.8
05	3	10	65	50	25.2	12	15	26	24	0.2	3.2	6.1	58	38	22	15.3	2	3.5	3x3.1	M4	1.5	9.5	6
06	8	12	80	63	22	15	17	35	27	0.2	3.5	6.1	72	46	18	19	2	4.5	3x3.1	M5	1.5	11.5	7.5
07	8	12	89	66.5	36	15	17	27	27	0.2	-	6.1	79.5	46	32	19	2	5	3x3.1	M5	1.5	11.5	-
08	16	18	100	80	24.5	20	20	42	32	0.2	4.3	8	90	60	20	24.7	2.5	5.3	3x4.1	M5	2	16	8.7
10	32	25	125	100	28	25	30	52	42	0.2	5	9	112	76	22	30	3	6.5	3x5.1	M6	2	19	11
11	32	25	143	105	44	25	30	47.6	42	0.2	-	9	127	76	38	30	3	7.5	3x5.1	M6	2	19	-
12	65	32	150	125	31	30	35	62	49	0.3	5.5	10	137	95	24	37.2	3.5	6.5	3x6.1	M6	2.5	24	13
13	65	32	165	125	39	30	35	52.4	49	0.3	-	10	149	95	33	37.2	3.5	10.2	3x6.1	M6	2.5	24	-
16	120	45	190	160	35	38	40	80	65	0.3	6	13	175	120	26	48	4	9	3x8.2	M8	9	30	16
20	240	60	230	200	41.4	48	60	100	92	0.5	7	16	215	158	30	59	5	9	3x10.2	M8	11	39	20

High torque (multi-pole) versions

Size	Torque TS (Nm)	Max P20 (w)	A1 H9	A2	B	C4	Max E2 H7	E4 H8	E5	G	H2	K	N1	N2	R2	S1	T	U1 x4	U2	U7	V	W1	W4
SZ06	12	12	80	63	28	15	17	35	27	0.2	3.5	6.1	72	46	24	19	2	4.5	3x3.1	M5	1.5	11.5	7.5
SZ08	30	21	100	80	32.5	20	20	42	32	0.2	4.3	8	90	60	27	24.7	2.5	5.3	3x4.1	M5	2	16	8.7
SZ10	50	21	125	100	35	25	30	52	42	0.2	5	9	112	76	29	30	3	6.5	3x5.1	M6	2	19	11

ISSUE 003